NASA CONTRACTOR REPORT

NASA CR-2520

NASA CR-2520

AERODYNAMIC DESIGN AND ANALYSIS SYSTEM FOR SUPERSONIC AIRCRAFT

Part 1 - General Description and Theoretical Development

W. D. Middleton and J. L. Lundry

Prepared by
BOEING COMMERCIAL AIRPLANE COMPANY
Seattle, Wash. 98124
for Langley Research Center

NATIONAL AERONAUTICS AND SPACE ADMINISTRATION • WASHINGTON, D. C. • MARCH 1975

1. Report No.	2. Government Accession No.	3. Recipient's Catalog No.
NASA CR-2520		

4. Title and Subtitle	5. Report Date
Aerodynamic Design and Analysis System for Supersonic Aircraft. Part 1--General Description and Theoretical Development	March 1975
	6. Performing Organization Code

7. Author(s)	8. Performing Organization Report No.
W. D. Middleton and J. L. Lundry	D6-41768
	10. Work Unit No.

9. Performing Organization Name and Address	11. Contract or Grant No.
Boeing Commercial Airplane Company P.O. Box 3707 Seattle, Washington 98124	NAS1-12052
	13. Type of Report and Period Covered Contractor Report Jan. 1973--Nov. 1974

12. Sponsoring Agency Name and Address	14. Sponsoring Agency Code
National Aeronautics and Space Administration Washington, D.C. 20546	

15. Supplementary Notes

One of three final reports

16. Abstract

An integrated system of computer programs has been developed for the design and analysis of supersonic configurations. The system uses linearized theory methods for the calculation of surface pressures and supersonic area rule concepts in combination with linearized theory for calculation of aerodynamic force coefficients. Interactive graphics are optional at the user's request.

The description of the design and analysis system is broken into three parts:

Part 1--General Description and Theoretical Development
Part 2--User's Manual
Part 3--Computer Program Description

This part presents a general description of the system and describes the theoretical methods used.

17. Key Words (Suggested by Author(s))	18. Distribution Statement
Wing design Configuration analysis Wave drag Pressure distribution	Unclassified--Unlimited New Subject Category 02

19. Security Classif. (of this report)	20. Security Classif. (of this page)	21. No. of Pages	22. Price*
Unclassified	Unclassified	78	$4.75

*For sale by the National Technical Information Service, Springfield, Virginia 22151

CONTENTS

Page Intentionally Left Blank

AERODYNAMIC DESIGN AND ANALYSIS SYSTEM FOR SUPERSONIC AIRCRAFT

PART 1 - GENERAL DESCRIPTION AND THEORETICAL DEVELOPMENT

W. D. Middleton and J. L. Lundry
Boeing Commercial Airplane Company

1.0 SUMMARY

An integrated system of computer programs has been developed for the design and analysis of supersonic configurations. The system uses linearized theory methods for the calculation of surface pressures and supersonic area rule concepts in combination with linearized theory for calculation of aerodynamic force coefficients. Interactive graphics are optional at the user's request.

The integrated system consists of an executive "driver" and seven basic computer programs including a geometry input module, which are used to build up the force coefficients of a selected configuration.

The description of the design and analysis system is broken into three parts:

Part 1 - General Description and Theoretical Development
Part 2 - User's Manual
Part 3 - Computer Program Description

This part presents a general description of the system and describes the theoretical methods used.

2.0 INTRODUCTION

Over a period of years, NASA-Langley has developed a basic computerized series of supersonic design and analysis methods for aerodynamic configuration studies (reference 1). The methods are characterized by their reliability in use and input simplicity.

The Boeing Company has extended this basic series of methods and combined them into an integrated system of computer programs. The extensions to the methods provide several new features:

- Addition of a near-field (thickness pressure) wave drag program, to complement the existing supersonic area rule program.
- Improved modeling of fuselage in lifting surface design and analysis programs.
- Addition of configuration-dependent loadings in wing design program, so that the wing design is performed in the presence of fuselage and nacelle effects.
- Addition of pressure limiting terms in the lifting pressure programs, to constrain the linear theory solution.
- Optional CRT displays of selected program input and output data and provisions for limited user editing and intervention.

A plot module is included in the system to produce configuration drawings, and a common geometry module is used to permit a single geometry input for all programs.

The basis of the system is supersonic linearized theory, modified in two respects:

- The "Whitham" correction to disturbance positioning is used in the propagation of body pressure fields.
- The wing lifting pressure modules contain an optional limiting pressure feature to control the permissable level of upper surface pressure coefficient.

Superposition is used to build up the theoretical force coefficients of a selected configuration.

The goals of the integrated system have been to develop an easily used supersonic design and analysis capability, with recognition of the need for constraints on linear theory methods to provide

physical realism, and with inclusion of interactive display for increased design control over optimization cycles.

3.0 SYMBOLS

A	element fraction
A_i	load strength factor
A(x)	cross sectional area at x
B	trailing edge element fraction
$\bar{c}$	pitching moment reference length
C	wing tip element fraction
c	chord
C_D	drag coefficient, D/qS
C_F	skin friction coefficient
C_L	lift coefficient, lift/qS
C_m	pitching moment coefficient, pitching moment/qSc
C_{mo}	pitching moment coefficient at zero lift
C_p	local pressure coefficient, $(p - p_\infty)/q$
ΔC_p	lifting pressure coefficient (lower surface pressure coefficient minus upper surface pressure coefficient)
D	drag force
F(y)	Whitham function
h(Z)	decay function for F(y) calculation
k	Mach number parameter
L	grid element variable in x(lengthwise) direction
M	Mach number
N	grid element variable in spanwise direction
p	pressure
q	dynamic pressure, $.7\ p_\infty\ M^2$
R	body radius
$\bar{R}$	influence function

r	radial distance to point in flow field
S	reference area or cross-sectional area (figure 4.3-3)
T	temperature
t	variable of integration (figure 4.3-4)
U	free stream velocity
u	x perturbation velocity
W(Z)	body pressure decay function
w	upwash
x	lengthwise variable
y	span station or distance variable
z	vertical variable
Z	decay function parameter
α	angle of attack
ϵ	local fuselage camber angle
β	Mach number parameter = $\sqrt{M^2 - 1}$
ξ	x variable of integration
λ	surface shape (equation 13) or Lagrange multiplier (figure 4.4-4)
η	spanwise variable of integration
ρ	density
ϕ	velocity potential
θ	radial angle variable
τ	region of influence
μ	dynamic viscosity coefficient

Subscripts:

∞	free stream conditions
i	incompressible condition (equation 5)

i,j	loading numbers (equation 31)
t	tilted lengthwise variable (figure 4.3-5)

Superscripts:

'	reference temperature condition (equation 2) or first derivative with respect to x
"	second derivative with respect to x
*	field point grid element

4.0 DISCUSSION

The integrated supersonic design and analysis system is shown schematically in figure 4.0-1. It consists of an executive "driver" and seven basic computer programs. The individual programs, or modules, provide data for configuration design or analysis as follows:

- Skin friction is computed using turbulent flat plate theory.

- Wave drag is calculated from either far-field (supersonic area rule) or near-field (surface pressure integration) methods. The far-field method is used for wave drag coefficient calculations and for fuselage optimization according to area rule concepts. The near-field method is used primarily as an analysis tool, where detailed pressure distributions are of interest.

- Lifting pressures, drag-due-to-lift, pitching moment and trim drag are computed from the lift analysis program, which breaks arbitrary wing/fuselage/canard/nacelles/horizontal tail configurations into a mosaic of "Mach-box" rectilinear elements which are employed in linear theory solutions. A complementary wing design and optimization program solves for the wing shape required to support an optimized pressure distribution at a specified flight condition.

- The plot module draws configuration pictures according to size and view inputs.

- The geometry module handles configuration geometry for the system.

- Interactive graphics, for data display or editing, are optional in the system at user's request.

Operating in the analysis mode, the force coefficients of a selected configuration are built up through superposition as shown in figure 4.0-2.

The entire design and analysis system is a single overlaid program. The executive level of the system controls module execution by means of special identification cards in the input data. Transfer of data in the system between modules is handled by disk storage and common blocks.

All configuration geometry is read (or updated) in the geometry module. Geometry inputs are patterned after those of the NASA-LRC configuration plotting program. All "paneling" of the

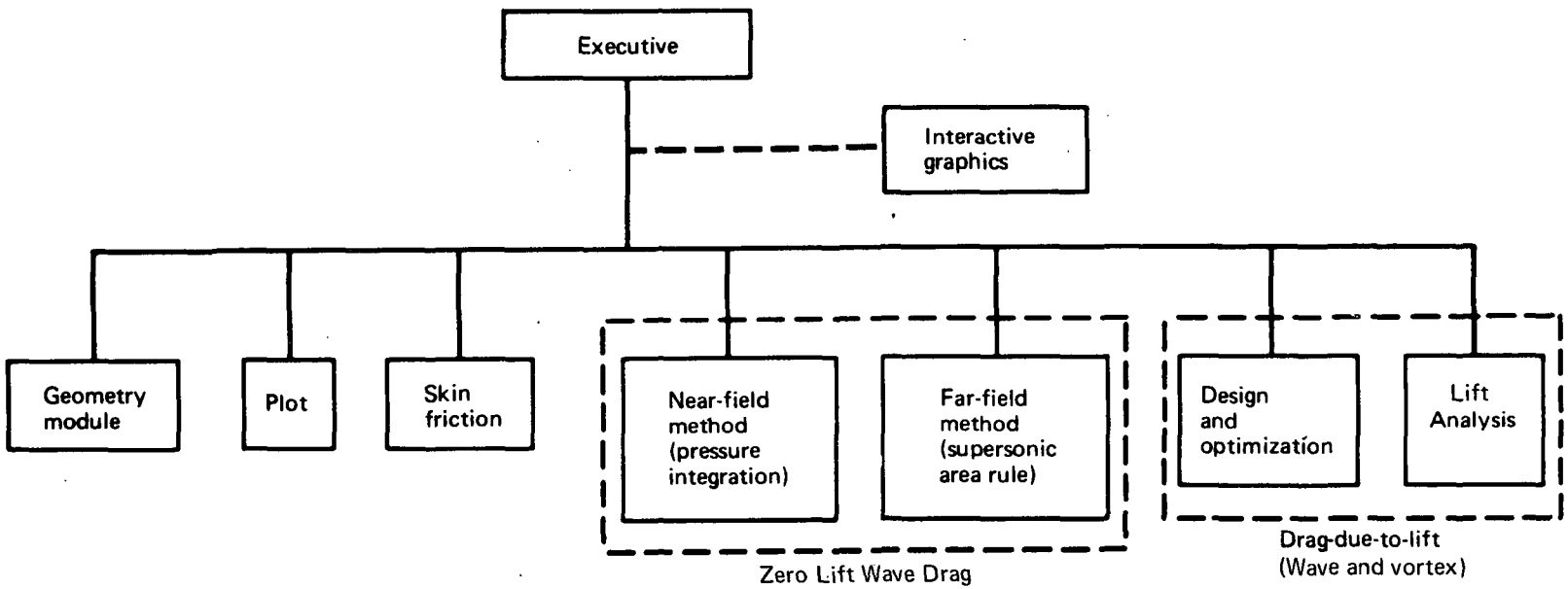

FIGURE 4.0-1.—INTEGRATED SUPERSONIC DESIGN AND ANALYSIS SYSTEM

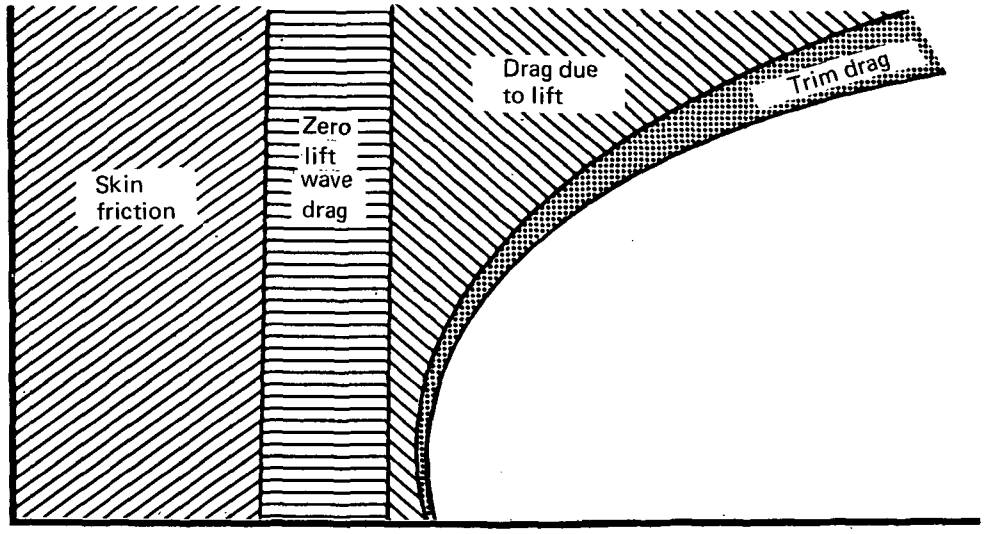

Drag

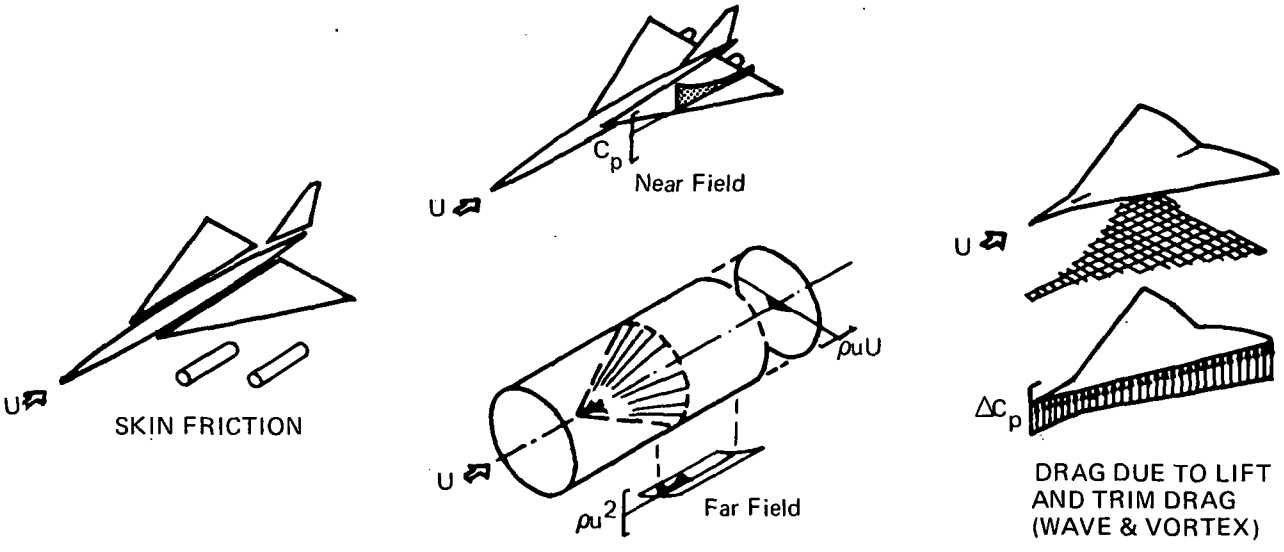

FIGURE 4.0-2.—DRAG BUILDUP

configuration for theoretical analyses is accomplished within the programs, and the user prepares only "drawing-type" geometry.

Additional data on system structure and input and output formats are presented in parts 2 and 3. The theoretical methods used in the modules are described in the remainder of this document.

4.1 Skin Friction Drag

The skin friction drag of an arbitrary configuration is calculated from the T′ method of reference 2. Smooth flat plate, adiabatic-wall, and turbulent boundary layer conditions are assumed, with transition assumed to occur at the leading edge of each configuration component.

The theory and experimental verification of the T′ method are given in detail in reference 2. The essential elements of the method are presented in Appendix C of the reference, and are summarized here for completeness.

The T′ method is based on the calculation of a compressible skin friction coefficient, C_F, from a reference skin friction coefficient, C_F', for a selected Mach number, M_∞, Reynolds number, R_∞, and adiabatic wall temperature, T_W. (The subscript ∞ is used throughout to denote free stream conditions).

The wall temperature ratio, T_W/T_∞, is calculated from one-dimensional relationships assuming a wall recovery factor of .89.

$$\frac{T_W}{T_\infty} = 1 + 0.178\, M_\infty^2 \tag{1}$$

The prime superscript (T', R', etc.,) refers to conditions at which incompressible flow relations must be evaluated in order to represent compressible flow. Sommer and Short in reference 2 obtained the key relationship

$$\frac{T'}{T_\infty} = 1 + 0.035\, M_\infty^2 + 0.45\left(\frac{T_W}{T_\infty} - 1\right) \tag{2}$$

The Reynolds number relationship is

$$\frac{R'}{R_\infty} = \frac{1}{\left(\frac{T'}{T_\infty}\right)\left(\frac{\mu'}{\mu_\infty}\right)} \tag{3}$$

where the viscosity ratio is given by the Sutherland equation

$$\frac{\mu'}{\mu_\infty} = \left(\frac{T'}{T_\infty}\right)^{1.5} \left(\frac{T_\infty + 216}{T' + 216}\right) \tag{4}$$

with T in degrees Rankine.

The incompressible skin friction coefficient is given by the Karman-Schoenherr equation

$$\frac{0.242}{\sqrt{C_{F_i}}} = \log_{10}\left(C_{F_i} R_i\right) \tag{5}$$

which gives the corresponding relationship based on the T' analogy:

$$\frac{0.242}{\sqrt{C_F'}} = \log_{10}\left(C_F' R'\right) \tag{6}$$

This equation is solved iteratively for C_F' . The desired compressible skin friction coefficient is obtained from C_F' by

$$C_F = C_F' \left(T_\infty/T'\right) \tag{7}$$

Most of the skin friction program is involved with computing wetted areas and reference lengths for the configuration. Components which may exhibit large variations in reference length (such as the wing, tail, canard etc.,) are broken into strips in order to calculate C_F accurately.

4.2 Far-Field Wave Drag

The far-field wave drag program computes the zero lift wave drag of an arbitrary configuration by means of the supersonic area rule. A description of the program has been given in reference 3, and is summarized here. The method assumes not only an integrated total lift of zero, but local lift everywhere zero, and thus includes none of the wave drag contribution associated with the generation of lift.

The supersonic area rule is a generalization of the transonic area rule, which states that the transonic wave drag of an aircraft is essentially the same as the wave drag of an equivalent body of revolution having the same cross-sectional area distribution. In the supersonic area rule procedure, several equivalent bodies of revolution are produced by passing a series of parallel cutting planes through the configuration, as shown below. The cutting

planes are inclined with respect to the aircraft axis at the Mach angle μ , and a single equivalent body is produced for the series of cutting planes at a constant azimuthal angle, θ . The area of the equivalent body at each station is the projection of the area intercepted by the cutting plane onto a plane normal to the aircraft axis.

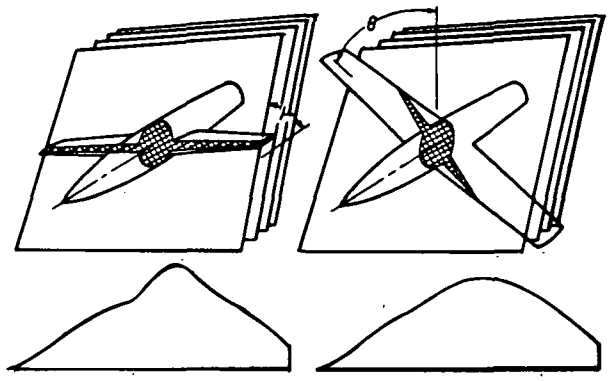

The wave drag of each equivalent body is calculated from the von Karman slender-body formula (reference 4), which gives the drag as a function of the free stream conditions and equivalent-body area distribution.

$$D(\theta) = -\frac{\rho U_\infty^2}{4\pi} \int_0^\ell \int_0^\ell A''(x_1)\, A''(x_2) \log |x_1 - x_2|\, dx_1\, dx_2 \qquad (8)$$

where X_1 and X_2 are lengthwise variables of integration and A" is the second derivative of the body area distribution.

The wave drag of the aircraft at a given Mach number is calculated from the integrated average of the equivalent-body wave drags.

$$D = \frac{1}{2\pi} \int_0^{2\pi} D(\theta)\, d\theta \qquad (9)$$

A useful feature of the supersonic area rule occurs in the optimization of a fuselage area distribution to minimize the wave drag of a wing-fuselage combination. According to Sheppard (reference 5), the wave drag of a wing-fuselage can be written as:

$$\frac{D}{q} = \left(\frac{D}{q}\right)_{\substack{\text{wing} \\ \text{+ body}}} + \left(\frac{D}{q}\right)_{\substack{\text{wing eq. body}}} - \left(\frac{D}{q}\right)_{\substack{\text{wing eq.} \\ \text{body}}} \qquad (10)$$

where the wing equivalent body is a body of revolution obtained by averaging from $\theta = 0$ to 2π all the projected areas intercepted by cutting planes passing through the wing for each X station.

Considering a wing-fuselage, then, and assuming that the wing geometry is fixed, both the first and third terms of equation 10 are fixed. This leaves optimization of the second term only, so that to design the minimum drag configuration, the fuselage must be contoured to produce a wing-equivalent-body-plus-fuselage having the shape of a minimum drag body of revolution.

The wave drag program uses the Eminton-Lord fairing through a discrete set of points, which defines the shape of a minimum drag body through the points. Using this fairing, and identifying a few "control-points" on the fuselage area definition, an optimized fuselage area definition may be obtained as the difference between the wing equivalent body and the combined wing-equivalent -body-plus-fuselage.

The wave drag program has mechanized this solution, and also includes the effects of nacelles, tail, etc., which are included similarly. The shape of the minimum drag fuselage area distribution, and the drag of the complete configuration including the minimum drag fuselage, may be calculated for each configuration input.

Because of the configuration generality that can be handled, the far-field program is the primary source of zero-lift wave drag coefficients in the design and analysis system. A complementary near-field program, more restricted in scope but which computes detailed thickness pressures, is described in the following section.

4.3 Near-Field Wave Drag

Isolated Component Pressures

The near-field wave drag program computes zero-lift thickness pressure distributions for an arbitrary wing-body-nacelle configuration in supersonic flow. The pressure distributions are integrated over the cross-sectional areas of the configuration to obtain the resultant drag force. Three basic calculations are performed to obtain the required pressure fields:

- Thickness pressure distribution for a wing of arbitrary section and planform.
- Thickness pressure distribution on surface of fuselage or nacelles.

- "Whitham" near-field calculations to define pressure distributions propagating from fuselage or nacelles.

Superposition is used to calculate the interference drag terms associated with the pressure field of a given component acting on the surfaces of the other components.

The surface pressure distributions calculated include some (from the nacelles) which contribute lift due to a non-symmetrical distribution of volume, so that the drag calculations which include these loadings contain wave drag due to lift contributions. However, by selection of program options and subtraction of certain drag contributions, a zero lift wave drag comparable to the far-field wave drag value may be obtained, as described on page 37.

Wing thickness pressures. - The surface pressure coefficient on the upper (or lower) surface of a flat-mean-line wing of symmetrical surface shape is obtained by first calculating the corresponding velocity potential, differentiating with respect to x (to get u), and then computing the pressure coefficient from the linear theory approximation, $C_p = -2u/U_\infty$.

The velocity potential computation, from reference 13, is:

$$\phi\,(x,y) = -\frac{1}{\pi}\iint_{\tau}\frac{\lambda\, d\eta\, d\xi}{\sqrt{(x-\xi)^2 - \beta^2(y-\eta)^2}} \qquad (11)$$

where $\phi(x,y)$ = velocity potential at a defined wing field point (x,y)
λ = surface slope (dz/dx) of wing section at a wing integration point
$\beta = \sqrt{M^2 - 1}$
ξ = x variable of integration
η = y variable of integration
τ = subscript denoting interval of integration (surface of the wing planform within the Mach forecone from x,y)

The wing thickness pressure coefficient is:

$$C_p\,(x,y) = \frac{p-p_\infty}{q_\infty} = -2\frac{u}{U_\infty} = -2\frac{\partial\phi\,(x,y)}{\partial x} \qquad (12)$$

where P = local pressure at x,y
p_∞ = free stream static pressure

u = x perturbation velocity
U_∞, q_∞ = free stream velocity and dynamic pressure

Integration of the velocity potential equation is performed by representing the wing as a grid of rectangular elements, and substituting a numerical summation for the integration. The wing element "Mach-box" system exactly follows the arrangement described in Section 4.4 (for the lifting pressure case) and is summarized in figure 4.3-1. The grid elements, identified by L and N, are defined such that L is numerically equal to x and N is numerically equal to βy, where x and βy take on only integer values. Partial grid elements along the wing leading and trailing edges are used to permit a closer approximation to the actual wing planform. The grid system of figure 4.3-1 is rather coarse for illustrative purposes; in actual usage, many more grid elements are employed.

With respect to a specified field point x,y, the upstream region of influence τ is approximated by the shaded grid elements in figure 4.3-1. Each of the shaded elements has associated with it an influence factor, $\bar{R}$, which relates the effect of the element and its surface slope to the total velocity potential at the field point.

The factor $\bar{R}$ is obtained by an approximate solution to Equation 11 as follows:

Let $y-\eta = u$ so that $du = -d\eta$

$$\phi(x,y) = \frac{1}{\pi}\iint_{\tau} \frac{\lambda \, du \, d\xi}{\sqrt{(x-\xi)^2 - \beta^2 u^2}} \tag{13}$$

Substituting an average value of $(x-\xi) = \overline{(x-\xi)}$ and integrating with respect to u,

$$\phi(x,y) = \frac{1}{\pi}\left[\frac{\lambda}{\beta} \sin^{-1} \frac{\beta u}{\overline{(x-\xi)}} \right]_{u_1}^{u_2} \tag{14}$$

Restoring $y - \eta = u$

$$\phi(x,y) = \frac{1}{\pi\beta}\left[\lambda \sin^{-1} \frac{\beta(y-\eta)}{\overline{(x-\xi)}} \right]_{\eta_1}^{\eta_2} \tag{15}$$

For a given grid element in the Mach forecone, the integration interval η_1 to η_2 gives

$$\beta(y-\eta_1) = N^* - N + 0.5$$
$$\beta(y-\eta_2) = N^* - N - 0.5$$

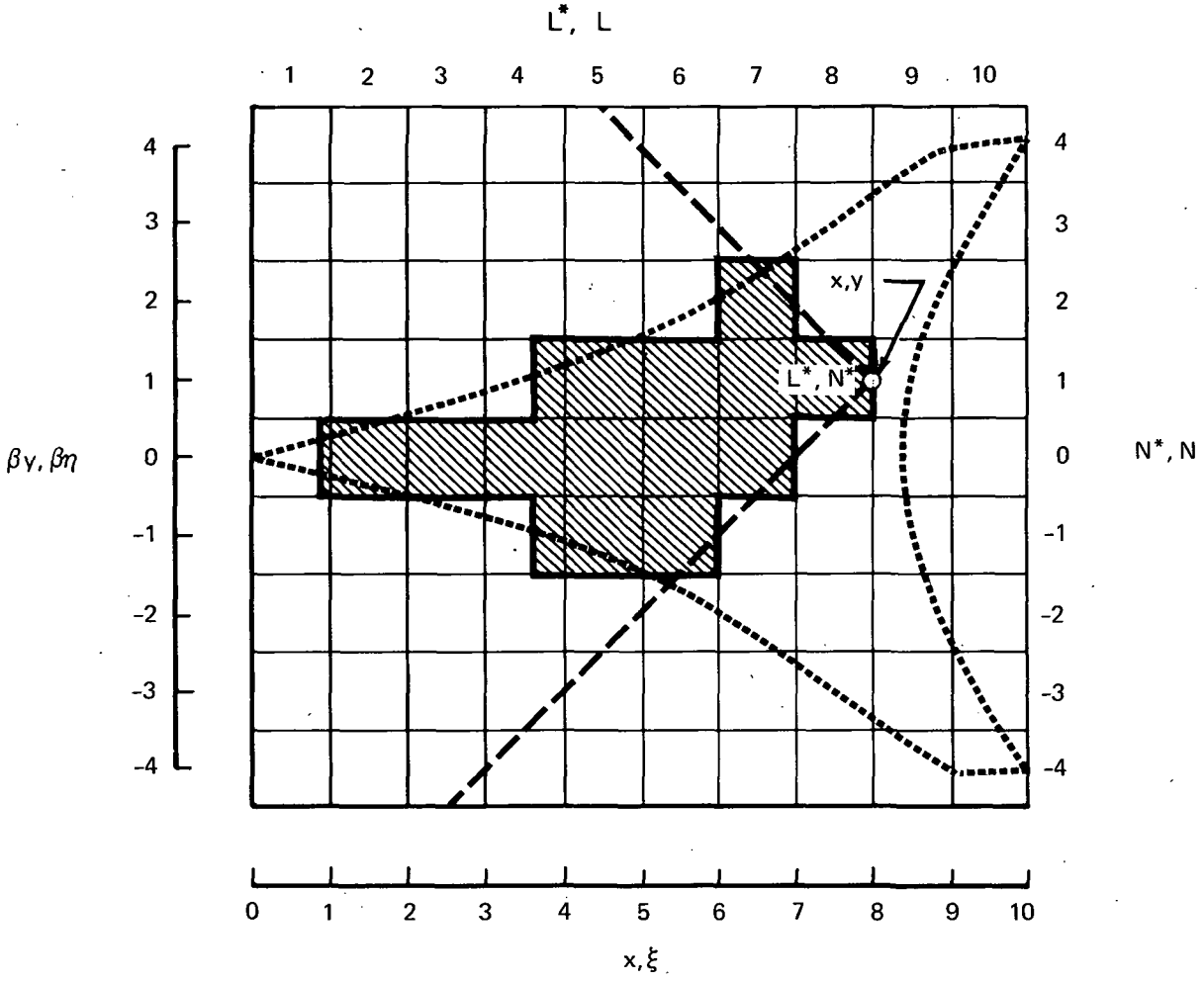

FIGURE 4.3-1.—WING COORDINATE SYSTEM

Also, $\overline{X-\xi} = L^* - L + 0.5$

L^* and N^* define the field point grid element and L and N define an element in the forecone. The numerical summation then becomes

$$\phi(x,y) = \frac{1}{\pi\beta}\sum_{\tau} \lambda_{L,N} \left[\sin^{-1}\frac{N^* - N - 0.5}{L^* - L + 0.5} - \sin^{-1}\frac{N^* - N + 0.5}{L^* - L + 0.5}\right] \qquad (16)$$

with $\bar{R}$ being the quantity between the brackets for the element (L,N).

The character of the $\bar{R}$ function is such that the sum of $\bar{R}$ for all elements across the Mach forecone at a constant L value is equal to $-\pi$. In considering the case of an infinite rectangular wing of constant thickness shape (wedge section), it is seen that the $-\pi$ summation must be the case. Since the ϕ function for successive L* rows is increased by

$$\frac{\lambda}{\pi\beta}[\Sigma\bar{R}]_{L=\text{const.}}$$

so that

$$\frac{\Delta\phi}{\Delta x} = \frac{\lambda}{\pi\beta}(-\pi) = -\frac{\lambda}{\beta}$$

and

$$C_p = -2\frac{\Delta\phi}{\Delta x} = 2\frac{\lambda}{\beta}$$

which is the established linear theory result. Values of $\bar{R}$ within the Mach forecone from a typical field element are presented in figure 4.3-2.

The computer program for the wing thickness pressure calculations sets up the wing grid system, defines the surface slope λ for each grid element, performs the summation for ϕ at selected field elements, and differentiates ϕ numerically to obtain C_p. Wave drag is obtained by summing the pressure coefficients times the corresponding surface slopes of the wing.

In the wing surface slope definition, slopes of the elements occupying space covered by the fuselage (if there is one) are set equal to zero to eliminate their drag contribution. Partial elements are used at the wing-body intersection to improve the geometry definition.

As was found to be the case in lifting surface programs involving the grid system used in the wing calculations, some oscillation in computed pressure coefficient values occurs. This has been

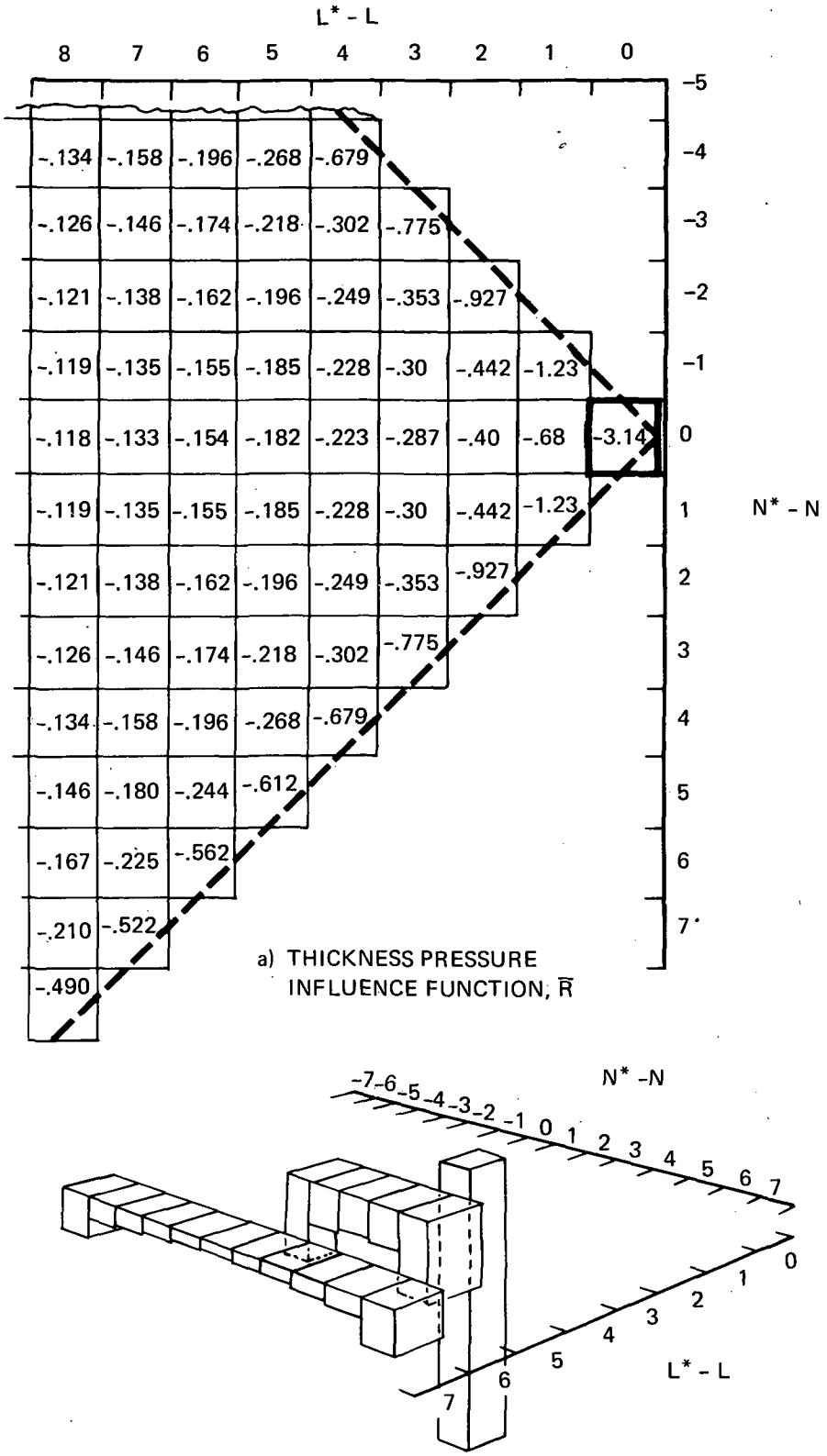

a) THICKNESS PRESSURE INFLUENCE FUNCTION, $\bar{R}$

b) REPRESENTATIVE INFLUENCE FACTOR CHARACTERISTICS

FIGURE 4.3-2.—THICKNESS PRESSURE INFLUENCE FUNCTION

suppressed by a smoothing of the calculated pressure coefficient values, using a 5 term equation of the form;

$$C_p = \frac{.333\,A_{L^*-2}\,C_{p_{L^*-2}} + .667\,A_{L^*-1}\,C_{p_{L^*-1}} + A_{L^*}C_{p_{L^*}} + .667\,C_{p_{L^*+1}} + .333\,C_{p_{L^*+2}}}{.333\,A_{L^*-2} + .667\,A_{L^*-1} + A_{L^*} + 1.0} \qquad (17)$$

where A = factor defining size of associated element (1 if whole element, fraction if not)

Fuselage and nacelle thickness pressures. - The pressure distribution on the surface of fuselage or nacelles is obtained from a method developed at the Boeing Company by R. M. Kulfan, based on the Lighthill theory of reference 6. The method is applicable to bodies having either smooth area distributions or bodies with slope discontinuities. As used in the near-field program, smooth area distributions are assumed except (if required) at the nose or aft end of the body. Open-nose bodies, such as nacelles, are permissable.

The solution technique is summarized in figure 4.3-3. An axial perturbation velocity is calculated which is a function of the body cross-sectional area growth (and radius distribution) and a decay function which relates area growth to its effect on a given field point.

The axial perturbation velocity, u, is given by

$$u(x) = -\frac{1}{2\pi}\int_0^x \frac{W(Z)}{\beta\, R_{(\xi)}}\, d\, S'_{(\xi)} \qquad (18)$$

where
- x = body field station
- $W(Z)$ = decay function
- ξ = x variable of integration
- Z = position function = $\frac{x-\xi}{\beta R_{(\xi)}}$
- $R_{(\xi)}$ = body radius at ξ
- $S'_{(\xi)}$ = first derivative of body cross-sectional area (S) at ξ

The pressure coefficient is calculated from one-dimensional flow relationships (rather than the simpler linear theory approximation), as shown in figure 4.3-3. The decay function, W(Z), is tabulated on page 23.

Fuselage and nacelle flow-field pressures. - The pressure field propagated by the fuselage or nacelles is calculated using the

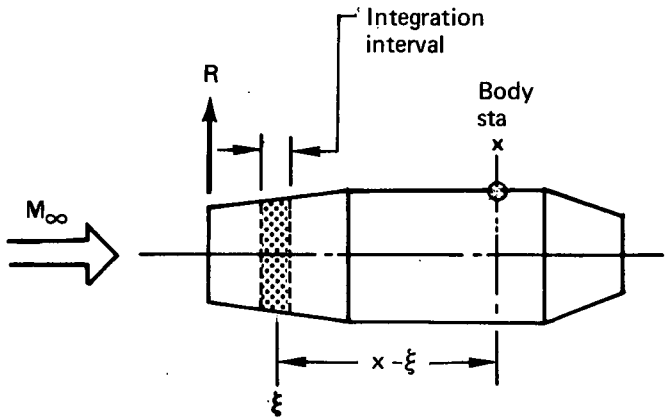

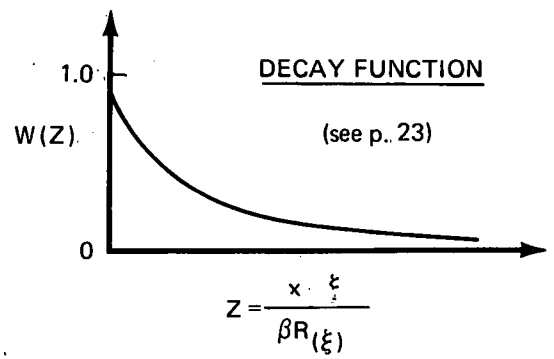

PERTURBATION VELOCITY

$$u(x) = -\frac{1}{2\pi}\int_0^x \frac{W(Z)}{\beta R_{(\xi)}}\, dS'_{(\xi)} \quad , \quad S = \text{cross-sectional area}$$

where:

dS' may include dS'_{smooth} and dS' discontinuous

$$u(x) = \Delta u_{(x)_{smooth}} + \Sigma\ \Delta u_{(x)_{disc}}$$

$$u(x)_{smooth} = -\frac{1}{2\pi}\int_0^x \frac{W(Z)}{\beta R_{(\xi)}}\left[\frac{dS'}{dx}\right] d\xi$$

Where integration excludes ds'_{disc}

$$\Delta u_{i(x)_{disc}} = -\left[\frac{\Delta R'(x_i)}{\beta}\right] W(Z_i)$$

PRESSURE COEFFICIENT

$$C_{p_{(x)}} = \frac{1}{0.7\, M_\infty^2}\left\{\left[1.0 + 0.2\, M_\infty^2\left(\left(1.0 + R'^2_{(x)}\right)\left(1.0 + u_{(x)}\right)^2 - 1.0\right)\right]^{3.5} - 1.0\right\}$$

FIGURE 4.3-3.–BODY SURFACE PRESSURES (LIGHTHILL THEORY)

DECAY FUNCTION

For body surface pressures. $Z = \frac{x - \xi}{\beta R_{(\xi)}}$, see fig. 4.3-3.

$\mathcal{Z}$	$W(\mathcal{Z})$
0	1.0
.1	.9518
.2	.907
.3	.8653
.4	.8265
.5	.7902
.6	.7562
.7	.7244
.8	.6946
.9	.6666
1.0	.6403
1.2	.5923
1.4	.5496
1.6	.5115
1.8	.4774
2.0	.4467
2.4	.3941
2.8	.3508
3.2	.3148
3.6	.2846
4.0	.2591
4.8	.2184
5.4	.1947
6.0	.1753
7.0	.1499
8.0	.1307
9.0	.1157
10.	.1037
12.	.0858
14.	.0731
16.	.0637
18.	.0564
20.	.0507
$>20.$	$1.0/\sqrt{1.0+\mathcal{Z}^2}$

Whitham solution of reference 7. This solution, which is converted to a method amenable to the digital computer in reference 8, calculates shock wave positions and strengths through a modification of linear theory results.

The Whitham solution begins with the calculation of a function, F(y), which is dependent on body geometry:

$$F(y) = \frac{1}{2\pi} \int_{o}^{y_{end}} \left[\frac{2}{\beta R_{(t)}} \right]^{\frac{1}{2}} h\,(Z)\, d\, S'_{(t)} \qquad (19)$$

where
- y = body field station
- $h(Z)$ = decay function (similar to body pressure calculation)
- t = y variable of integration
- Z = t position function
- $S'(t)$ = first derivative of body cross-sectional area (S) at t
- y_{end} = y at end of integration (see figure 4.3-4).

The solution for F(y) is very much like that of the body thickness pressure solution, with the exception that the integration is carried out to the point (y_{end}) at which the aft-running Mach line from the body centerline at y emerges from the body contour. The F(y) calculation is summarized in figure 4.3-4, and the decay function h(Z) is tabulated on page 27.

Development of the near-field pressure signature at a radial distance (r) from the body centerline is summarized in figure 4.3-5. The F(y) function is tilted, as shown, by displacing the F(y) function according to

$$\Delta y = k\sqrt{r}\, F(y) \qquad (20)$$

where

$$k = \frac{1.6973\, M^4}{\beta^{1.5}}$$

This process results in a double-valued pressure signature where shock waves are present, a situation which is corrected by an area-balancing technique. The area-balancing (shaded lobes are equal in area) defines shock wave locations and strengths. The resultant tilted/area-balanced signature is then converted to pressure coefficient by

$$C_p = \frac{p - p_\infty}{q_\infty} = \frac{2\, F(y)}{\sqrt{2\beta r}} \qquad (21)$$

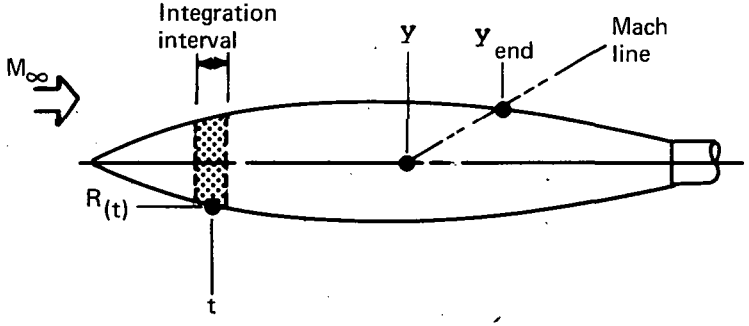

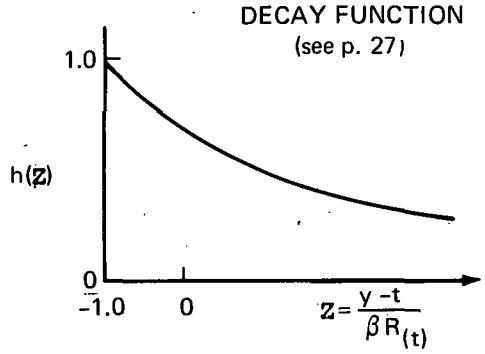

$$F(y) = \frac{1}{2\pi} \int_0^{y_{end}} \left[\frac{2}{\beta R_{(t)}} \right] h(Z)\, dS'_{(t)}$$

S = Cross-sectional area

PRESSURE COEFFICIENT

$$C_p = \frac{p - p_\infty}{q_\infty} = \frac{2F(y)}{\sqrt{2\beta r}}$$

where:

r = radial distance from body

F(y) function displaced, shock waves located as shown in fig. 4.3-5

FIGURE 4.3-4.—WHITHAM F(y) FUNCTION (NEAR-FIELD PRESSURE BASIS)

$k = \frac{1.6973\,M^4}{\beta^{1.5}}$, r = radial distance from body

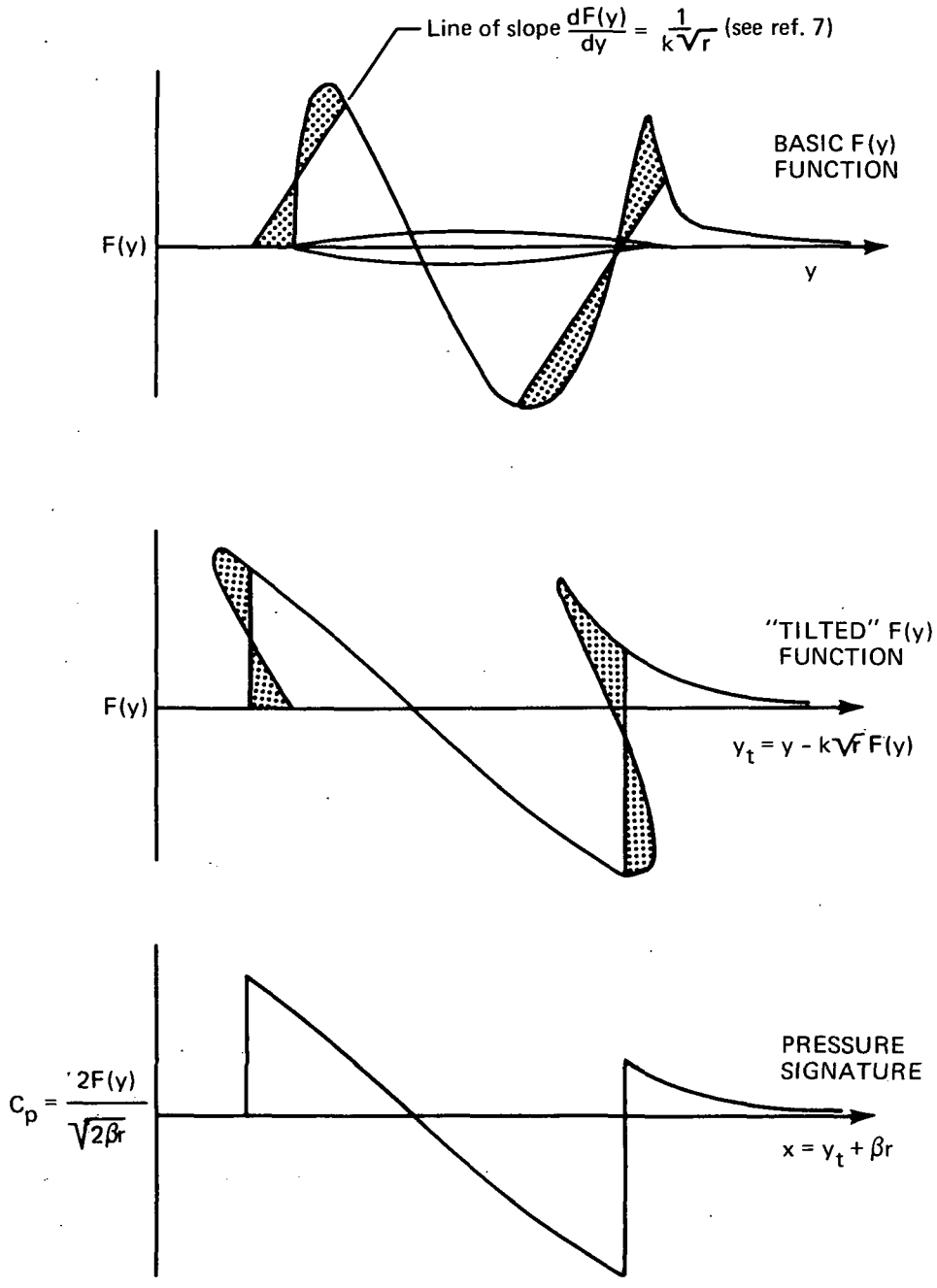

FIGURE 4.3-5.—DEVELOPMENT OF NEAR-FIELD PRESSURE SIGNATURE

DECAY FUNCTION

For F(y) calculation. $z = \frac{y - t}{\beta R_{(t)}}$, see fig. 4.3-4.

$\mathcal{Z}$	h($\mathcal{Z}$)
-1.0	1.0
-.9	.964
-.8	.929
-.7	.897
-.6	.868
-.5	.84
-.4	.814
-.3	.789
-.2	.766
-.1	.742
0	.72
.25	.674
.50	.633
.75	.597
1.0	.565
1.5	.511
2.0	.467
2.5	.431
3.0	.401
3.5	.375
4.0	.353
>4.0	$1.0/\sqrt{2\mathcal{Z}}$

The position of the pressure signature at radius (r) is then given by

$$x = y_t + \beta r \tag{22}$$

where x is the longitudinal distance from the body nose. The "tilting" thus produces a correction in pressure signature positioning, relative to simple translation along a Mach line, which is the result of the remarkable theory of reference 7.

Interference Calculations

The previous sections summarized the basic pressure calculations performed by the near-field wave drag program. Integration of the wing and fuselage or nacelle pressure distributions over their respective surfaces gives the "isolated" wave drags of the components. Interference drags are obtained by superposition; i.e., the pressure field of each component is imposed upon the surfaces of the other components to calculate the resultant interference forces.

The computer solution allows for up to 3 pairs of nacelles located external to the wing-fuselage (or 2 pairs plus a single nacelle at Y=0). The nacelles may be either above or below the wing (or both).

Wing-fuselage interference. - Fuselage-on-wing interference is obtained by calculating the near-field pressure signature from the fuselage at selected spanwise stations, and imposing them upon the corresponding wing sections as a bouyancy field. The spanwise stations are the same as those used in the isolated wing thickness pressure calculations.

Wing-on-fuselage interference is obtained by computing wing thickness pressures in the area occupied by the fuselage, after the wing surface slopes in the fuselage area have been set equal to zero. The thickness pressures thus calculated are "carry-over" pressures, and are imposed upon the fuselage surface slopes by transposing them aft along Mach lines to the fuselage. The fuselage area covered by the wing root is deleted from the interference term.

Typical results from wing-body calculations are presented in figure 4.3-6. The wing data, both isolated and fuselage-on-wing interference, are converted to section drag form.

$C_{D_{wing}} = 0.00113$ $C_{D_{wing\text{-}on\text{-}body}} = 0.00008$ $\Sigma C_{D_{wing\text{-}body}} = 0.00153$

$C_{D_{body}} = 0.00032$ $C_{D_{body\text{-}on\text{-}wing}} = -.000003$

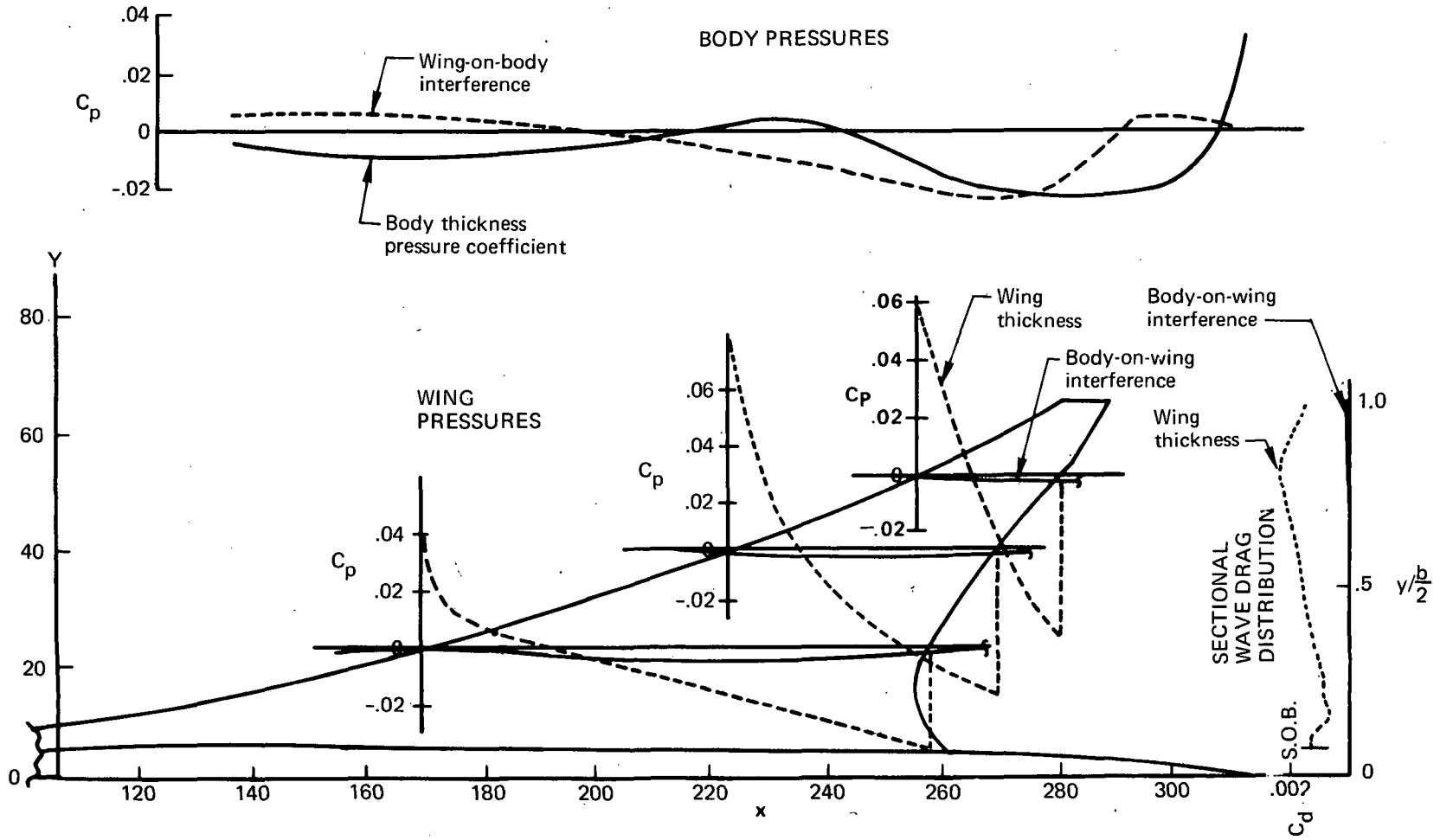

FIGURE 4.3-6.– WING-BODY SOLUTION, M = 2.6

Nacelle interference terms are calculated like the wing-body interference terms, with the provision that two alternate solutions may be specified for the nacelle-on-wing interference term. Available experimental data do not make it clear whether a "wrap" or "glance" solution, as shown in figure 4.3-7, is more correct. Since the nacelle-on-wing interference term is substantial, both solutions are available in the program (controlled by an input code).

The nacelle interference terms are calculated as follows:

Nacelle-on-wing term. - The nacelle pressure field acting on the wing is obtained by calculating nacelle pressure signatures at the same spanwise stations used for the wing thickness pressures (plus extra stations immediately adjacent to the nacelle centerlines), then defining a composite signature by summing together the contributions from all nacelles. The nacelle pressure coefficients are doubled to account for reflection from the wing surface.

In the case of nacelles both above and below the wing, separate nacelle pressure fields for nacelles below, and then above, the wing are calculated and then summed.

A unique feature of the near-field approach lies in the solution choices available, since the pressure signatures generated by a nacelle to act on the wing surface may be terminated on encountering another nacelle or may be allowed to pass undiminished around (or through) it. In the first case, the "glance" solution, the nacelle pressure field is assumed to reflect from other nacelles in such a way that the reflected field exerts no further influence upon the wing surface. In the second case, the "wrap" solution, the nacelle pressure field is assumed to propagate around the other nacelles as if no obstruction were offered, i.e., as if they were transparent to the pressure field.

A comparison of the theoretical nacelle pressure field with experimental data is presented in figures 4.3-8 and 4.3-9 at Mach numbers of 2.7 and 1.1. At $M = 2.7$, there is no difference between wrap and glance solutions. At $M = 1.1$, the solution choice appears to favor the glance approach except on the outboard wing. However, the experimental pressure points are too sparse to permit firm conclusions.

Nacelle-on-fuselage term. - The effect of the nacelles on the fuselage area distribution is built up by integrating each nacelle's pressure signature upon the fuselage area growth, with the provision that nacelles below the wing affect only the fuselage area below the wing in the region of the wing (and vice-versa for above-wing nacelles). In the fuselage region below the wing, or above the wing, the nacelle pressures are doubled to

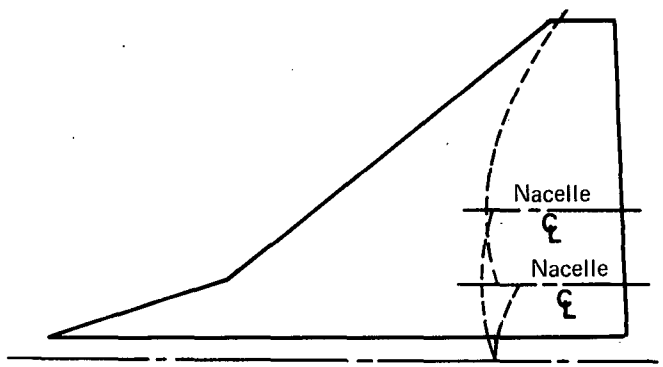

PRESSURES "GLANCE" AWAY FROM WING AT ADJACENT NACELLES

The nacelle pressure field and accompanying shock waves "glance" away from the wing when encountering adjacent nacelles. In application, the nacelle generated pressure field is terminated on encountering another nacelle.

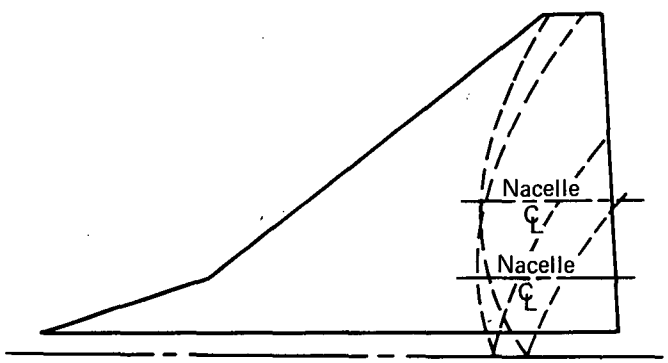

PRESSURES "WRAP" AROUND ADJACENT NACELLE

The nacelle pressure fields and accompanying shock waves "wrap" around adjacent nacelles. In application, the nacelle generated pressure field is allowed to pass through another nacelle as if it were transparent.

FIGURE 4.3-7.—NACELLE GENERATED WING PRESSURE FIELD CONCEPTS

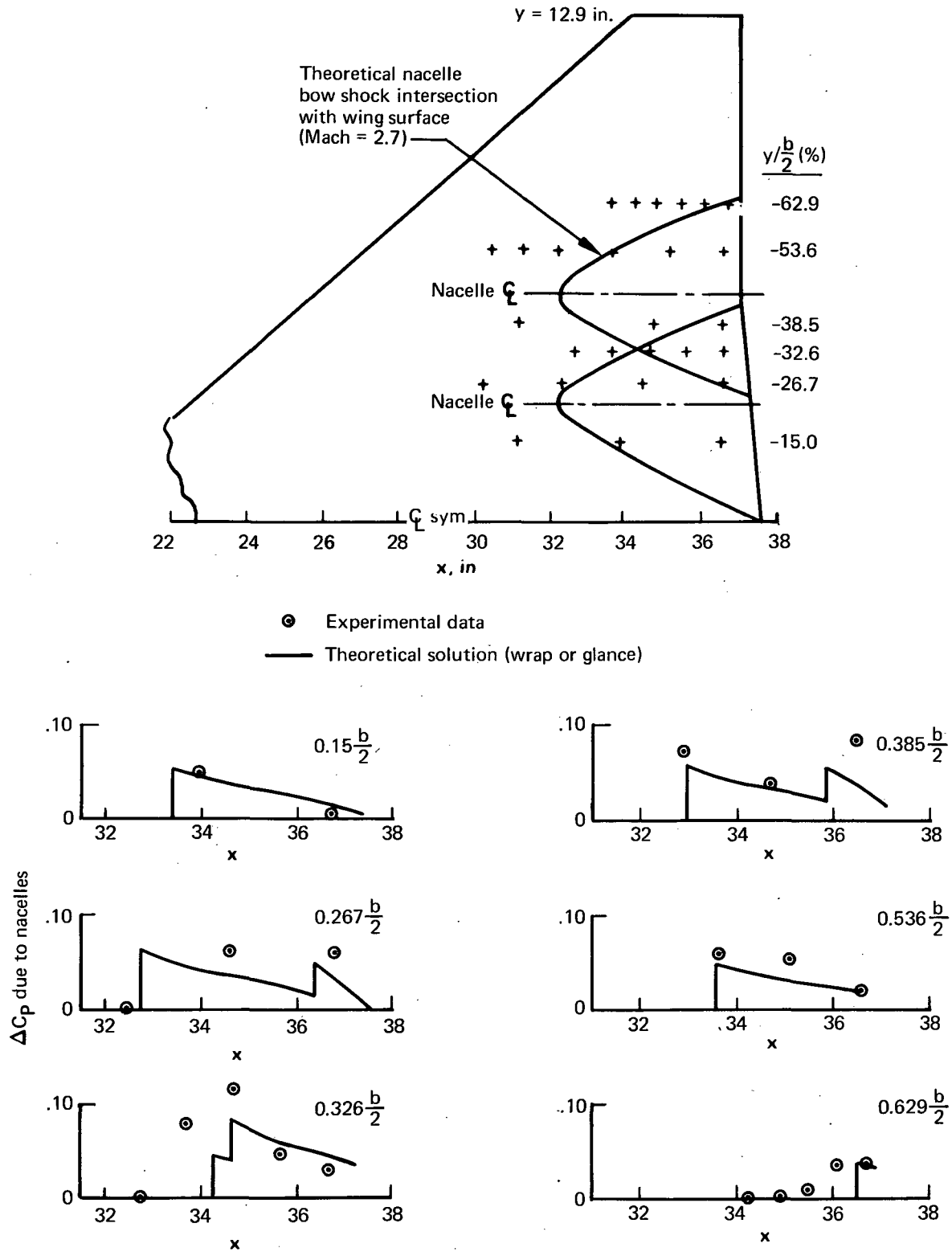

FIGURE 4.3-8.—NACELLE PRESSURE FIELD DATA, M = 2.7

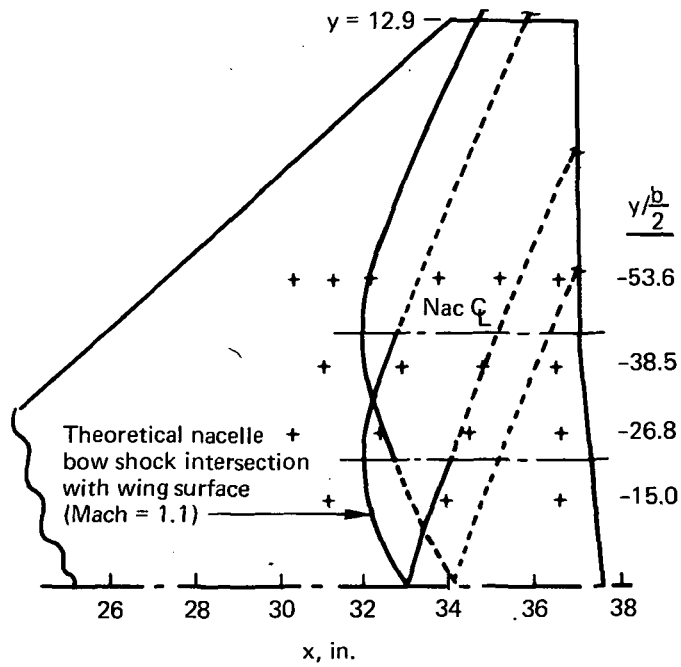

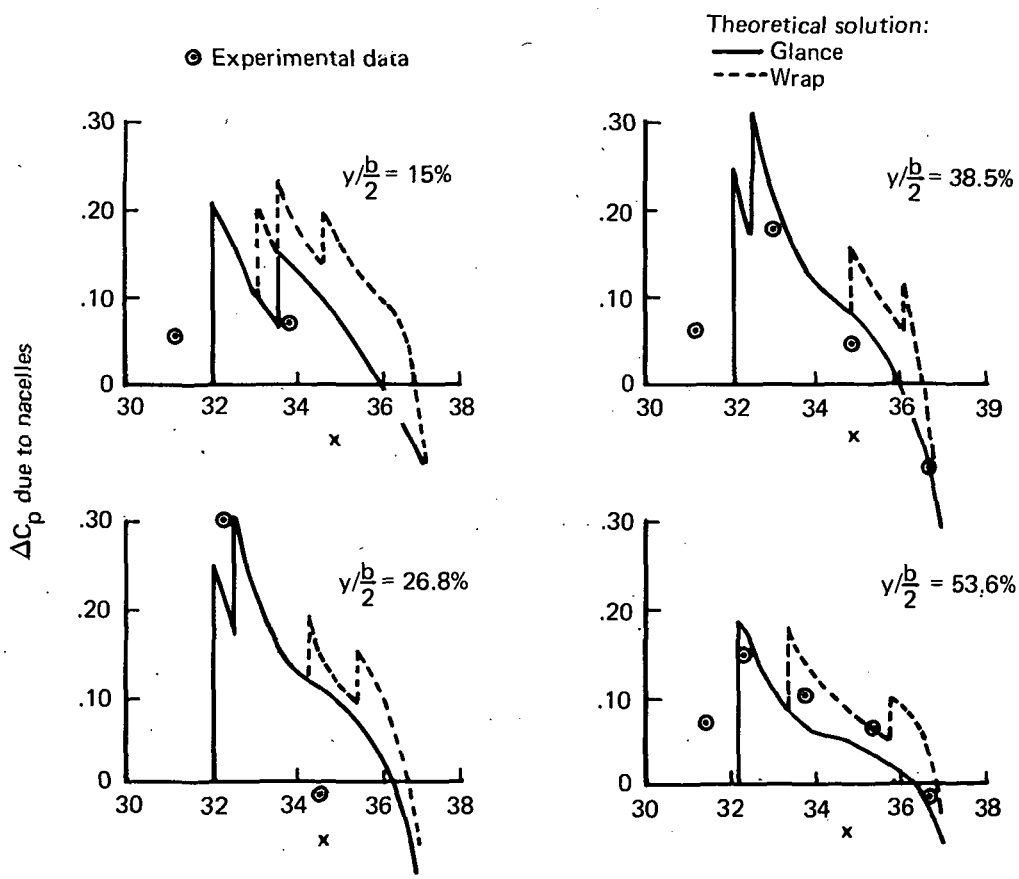

FIGURE 4.3-9.—NACELLE PRESSURE FIELD DATA, M = 1.1

account for reflection (as is done in the nacelle pressure field case).

Fuselage-on-nacelle term. - The fuselage pressure signature is imposed on each nacelle surface as a bouyancy force.

Wing-on-nacelle term. - Wing thickness pressures at span stations where nacelles are located are transferred aft along Mach lines from the wing surface to the nacelle centerline to obtain the buoyancy field acting on each nacelle.

Nacelle-on-nacelle term. - The interference term of other nacelles acting on a selected nacelle is calculated by building up the composite buoyancy field, and then imposing it upon the nacelle surface. In the case of nacelles on opposite sides of the wing, the pressure signatures are cut off where intercepted by the wing.

The nacelle-generated pressure field is assumed to pass undiminished around or through other nacelles that may be present when a particular nacelle pair interference term is being calculated much as in the "wrap" solution employed for nacelle on wing terms. The "wrap" or "glance" option is not provided in this case because of the generally negligible difference in results.

Nacelle image effects. - If the nacelle is located next to the wing (or body), an "image" nacelle is used to create the reflected buoyancy field. The reflected field is cut off forward or aft of the wing if the nacelle is not entirely under the wing.

The principal image effect is caused by the nacelle pressure field reflecting off the wing back onto itself. However, the reflected nacelle pressure field acting on other nacelles is also computed. This solution also utilizes an image nacelle representation, and the reflected signature is restricted to whatever part of the "real" signature encountered a reflecting surface.

Composite Thickness Pressure Signatures and Configuration Drag

Typical theoretical thickness pressure distributions acting on the configuration components are presented in figure 4.3-10. The net effect of these pressure signatures on drag is obtained by summing the various inputs and integrating them over the surface of the configuration. The corresponding drag terms are summarized in the data of figure 4.3-11.

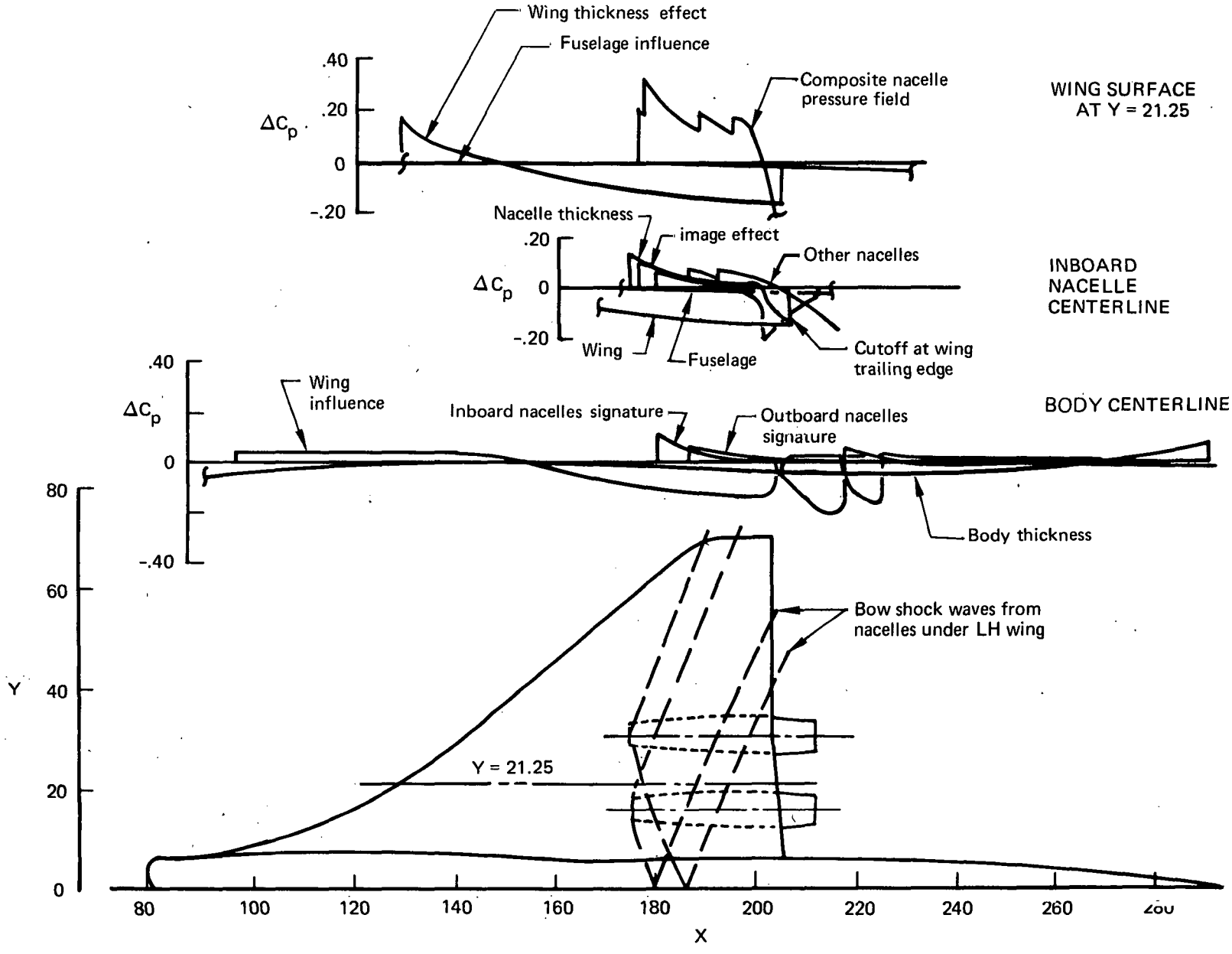

FIGURE 4.3-10.—NEAR-FIELD PRESSURE SIGNATURES, M = 1.1 "WRAP" SOLUTION

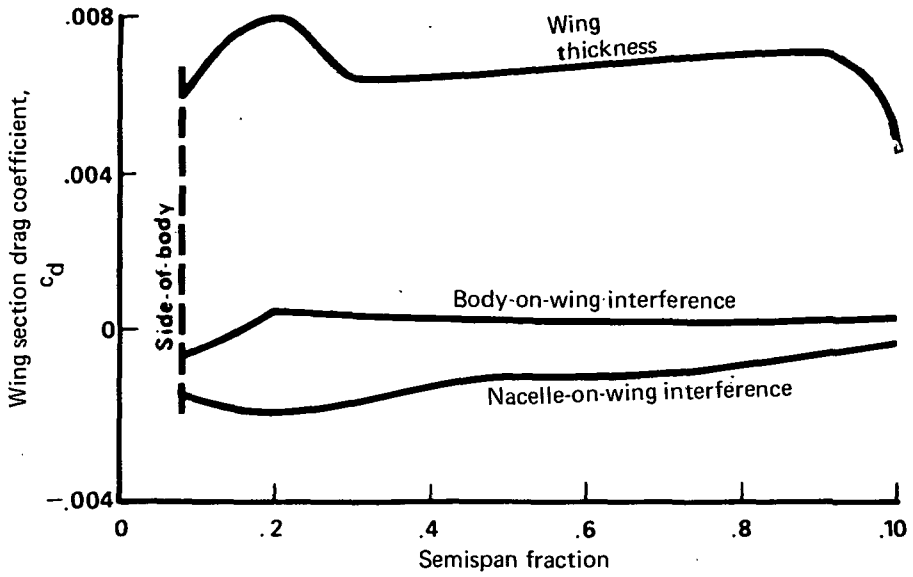

Wing-Body Terms

$C_{D_{wing}}$ = 0.00639

$C_{D_{body}}$ = 0.00072

$C_{D_{wing\text{-}on\text{-}body\ interference}}$ = −0.00013

$C_{D_{body\text{-}on\text{-}wing\ interference}}$ = 0.00013

Σ = 0.00711

Nacelle Terms

Isolated $C_{D_{wave}}$	0.00075	0.00075
Body-on-nacelle interference	-0.00002	0.00000
Nacelle-on-body interference	0.00005	0.00010
Nacelle-on-nacelle interference		
Direct	0.00034	0.00023
Image	0.00054	0.00046
Wing-on-nacelle interference	-0.00043	-0.00058
		-0.00156

$\Sigma C_{D_{nac}}$ = 0.00064

Σ Wing-body-nacelle $C_{D_{wave}}$ = 0.00775

FIGURE 4.3-11.—TYPICAL WAVE DRAG COEFFICIENT SUMMARY NEAR-FIELD PROGRAM, M = 1.1

The near-field wave drag program has three calculation features that have no direct counterpart in the far-field wave drag program. These are:

1) Wrap or glance solution for nacelle pressure field acting on wing. The wrap solution is nominally the same as the far-field solution.

2) Nacelle image effects. Because of the transparency assumption of the far-field program pressure propagation, nacelle pressures do not reflect off adjacent surfaces. (Through addition and subtraction of separate calculations involving "image" nacelles, however, comparable drag data can be generated using the far-field program.)

3) Above- or below- wing fuselage area separation in the nacelle-on-fuselage term. Directly comparable results are obtained only for mid-wing configurations.

Using the "wrap" solution, a mid-wing arrangement, and subtracting the nacelle image drag terms, a direct comparison between near-field and far-field program drag calculations can be made.

4.4 Drag-Due-to-Lift (Design and Analysis)

The wing design and lift analysis modules are separate lifting surface methods which solve the direct or inverse problems of:

- Design - to define the wing camber surface shape required to produce a selected lifting pressure distribution. The wing design program includes methods for defining an optimum (least drag) pressure distribution.

- Lift analysis - to define the lifting pressure distribution acting on a given wing camber surface, and calculate the associated force coefficients.

Originally, these programs were developed to utilize the "Mach-box" method of wing representation and evaluation of linear theory integral equations (references 9 through 11). In the Mach - box method, the wing is replaced by a grid of small rectilinear elements. Since many elements (in the thousands) can be used, a detailed description of complicated surface shapes, with associated computational accuracy, is possible.

The wing design and lift analysis programs have been expanded several times to add features (e.g., reference 11) and were recently reviewed in reference 12. The discussion of the

aerodynamic theory of the Mach-box method in reference 12 is quite detailed, and is summarized here for completeness. The numerical method for the "direct" case of wing design and optimization is given first, followed by the inverse case of lift analysis on page 50.

Design Case

Camber surface for a given loading. - A typical wing planform described by a rectangular cartesian coordinate system is illustrated in figure 4.4-1. The y coordinate has been multiplied by the Mach number parameter $\beta = \sqrt{M^2 - 1}$ for convenience in mathematical manipulations.

For a wing of zero thickness lying essentially in the z=0 plane, linearized theory for supersonic flow defines the wing surface shape necessary to support a specified lift distribution by the integral equation (23)

$$\frac{\partial z_c}{\partial x}(x,y) = \frac{-\beta}{4}\Delta C_p(x,y) + \frac{1}{4\pi}\iint d\xi \iint_{\tau} \frac{(x-\xi)\,\Delta C_p(\xi,\eta)\,d\eta}{(y-\eta)^2\sqrt{(x-\xi)^2 - \beta^2(y-\eta)^2}}$$

which is slightly modified form of equation (77a) of reference 13. With respect to a specified field point x, y, the upstream region of influence, τ , enclosed by the Mach forecone is shown by the shaded area.

Equation 23 may be rewritten into an influence function form by introducing the factor $\bar{R}$, such that

$$\frac{\partial z_c}{\partial x}(x,y) = \frac{-\beta}{4}\Delta C_p(x,y) + \frac{\beta}{4\pi}\iint d\xi \iint_{\tau} \bar{R}(x-\xi,y-\eta)\,\Delta C_p(\xi,\eta)\,d\beta\eta \qquad (24)$$

where $\bar{R}$ is defined as

$$\bar{R}(x-\xi,y-\eta) = \frac{x-\xi}{\beta^2(y-\eta)^2\sqrt{(x-\xi)^2 - \beta^2(y-\eta)^2}} \qquad (25)$$

$\bar{R}$ is a function relating the local loading at point ξ , η to its influence in determining the downwash (or upwash) at the field point.

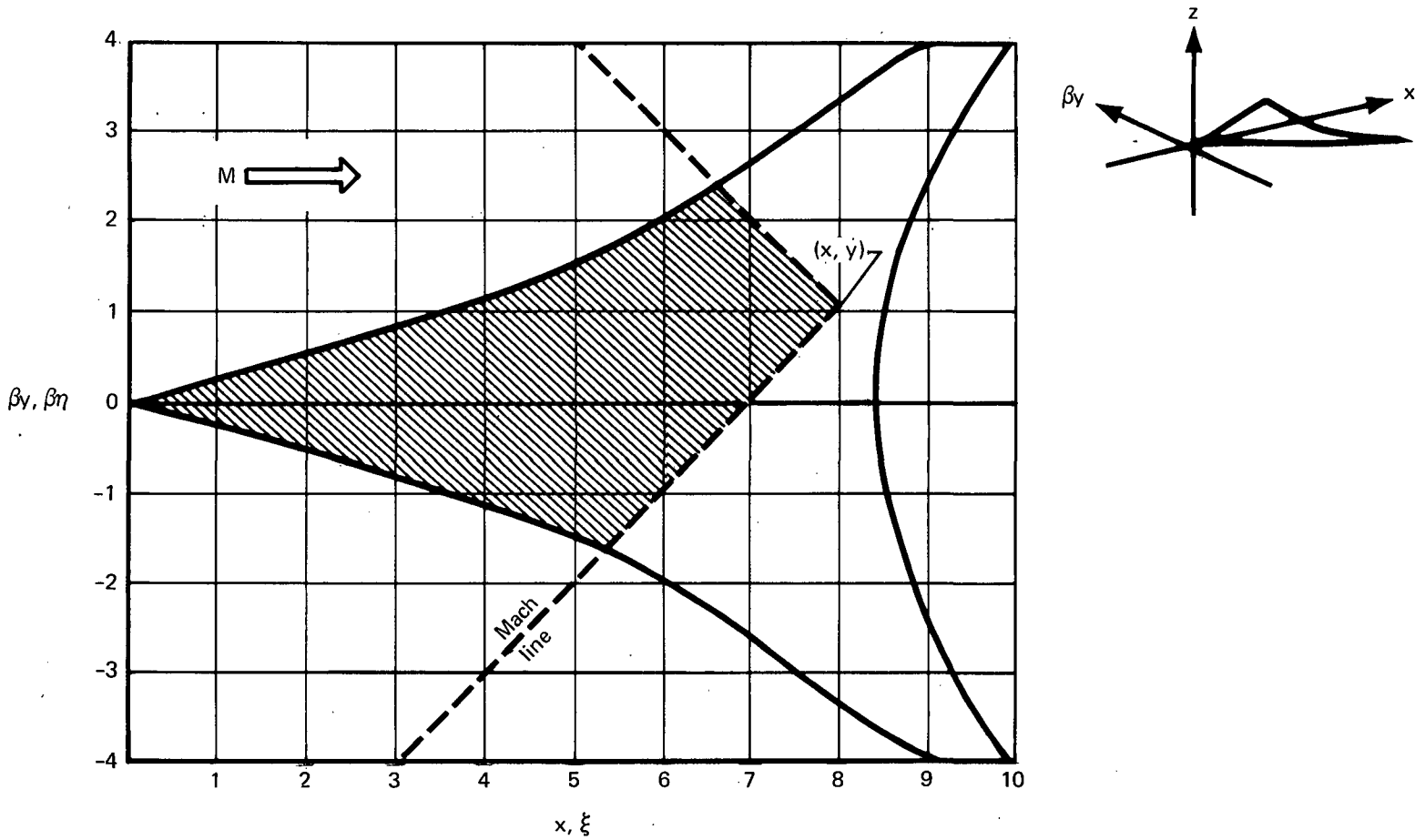

FIGURE 4.4-1.—CARTESIAN COORDINATE SYSTEM

For the numerical evaluation of this integral, the wing is replaced by the grid system of figure 4.4-2. The grid elements, identified by L and N, are defined such that L is equal to X and N is equal to β_y, where X and β_y take on only integer values. Partial grid elements along the wing leading and trailing edges are used to permit a closer approximation to the actual wing planform. The grid system of figure 4.4-2 is rather coarse for illustrative purposes. In actual usage, many grid elements are employed.

In the grid system, the field point x, y is located at the aft midpoint of a field point element L*, N*, and the region of integration, τ, is approximated by the shaded grid elements.

The integration required by equation 24 is performed for each element within the Mach forecone, considering ΔC_p constant over the element and using an average value of $X-\xi = L^*-L+.5$. The resulting expression, derived in reference 12, is the factor $\bar{R}$ which is the value of the influence function for an element L, N:

$$\bar{R}(L^*-L,N^*-N) = \frac{\sqrt{(L^* - L + 0.5)^2 - (N^* - N - 0.5)^2}}{(L^* - L + 0.5)(N^* - N - 0.5)} - \frac{\sqrt{(L^* - L + 0.5)^2 - (N^* - N + 0.5)^2}}{(L^* - L + 0.5)(N^* - N + 0.5)} \tag{26}$$

The integral equation 23 may then be replaced by the summation given below, where the summation includes all elements within the forecone and on the wing planform. The factors A, B, and C are element fractions for the wing leading edge, trailing edge, and wing tip, respectively, to allow for partial elements at those locations.

$$\frac{\partial z_c}{\partial x}(L^*,N^*) = \frac{-\beta}{4}\Delta C_p(L^*,N^*) + \frac{\beta}{4\pi}\sum_{\tau}\bar{R}(L^*-L,N^*-N)\,A(L,N)\,B(L,N)\,C(L,N)\,\Delta C_p(L,N) \tag{27}$$

The character of the $\bar{R}$ function is such that, for a given L*-L set of elements within the forecone, the sum of the $\bar{R}$ values is zero, the single negative value at N*-N=0 balancing all the others (see figure 4.4-3). At L* =L, where there is only one element in the summation, the $\bar{R}$ value is zero.

The physical significance of this $\bar{R}$ variation is that (for positive lift), all elements directly ahead of the field point element contribute only downwash and all other elements contribute upwash. An element at the leading edge near the wing tip of a subsonic leading edge wing, therefore, sees a concentrated upwash field. It is this upwash field that makes the subsonic leading edge twisted and cambered wing attractive from the standpoint of

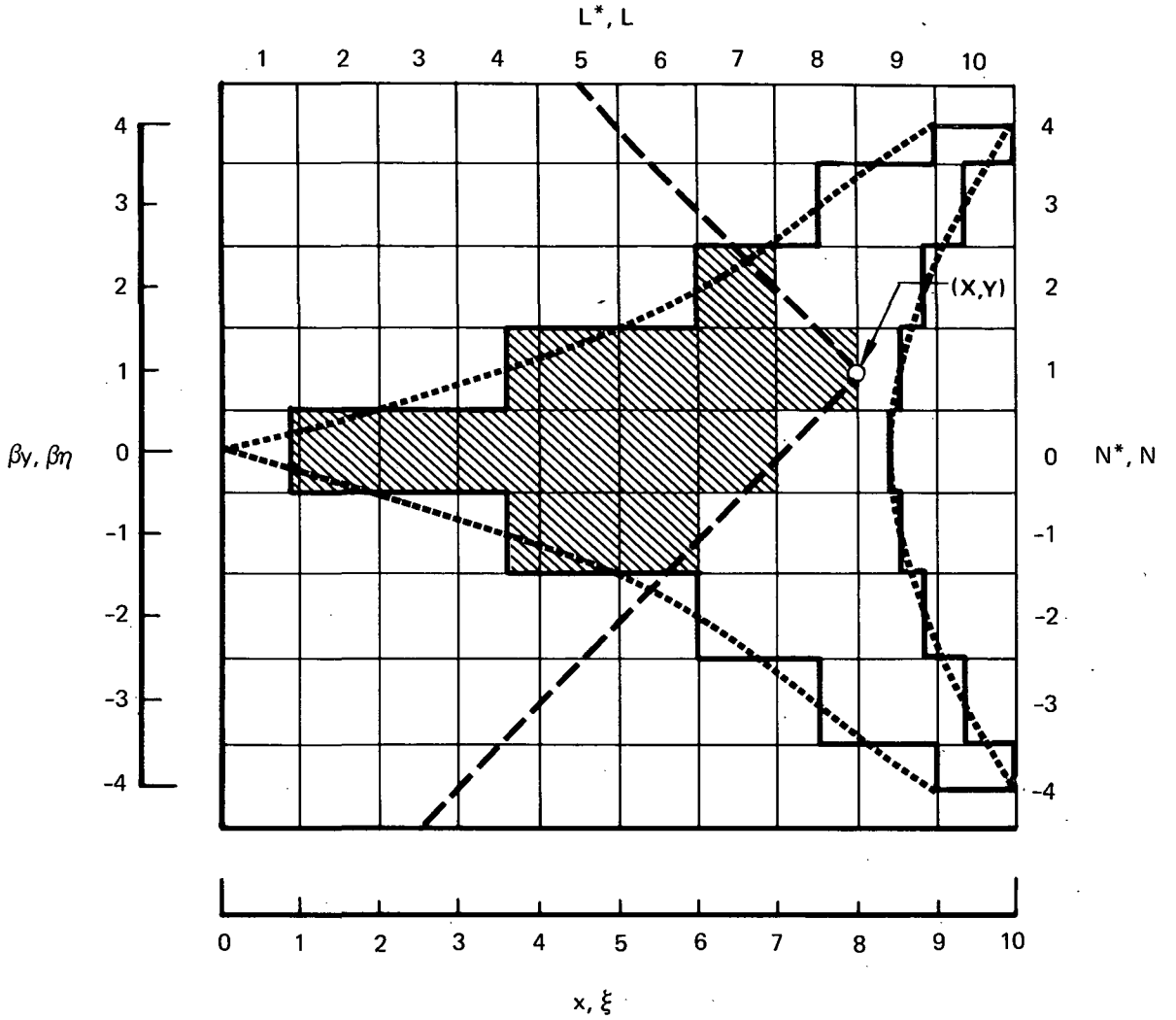

FIGURE 4.4-2.– GRID SYSTEM USED IN NUMERICAL SOLUTION

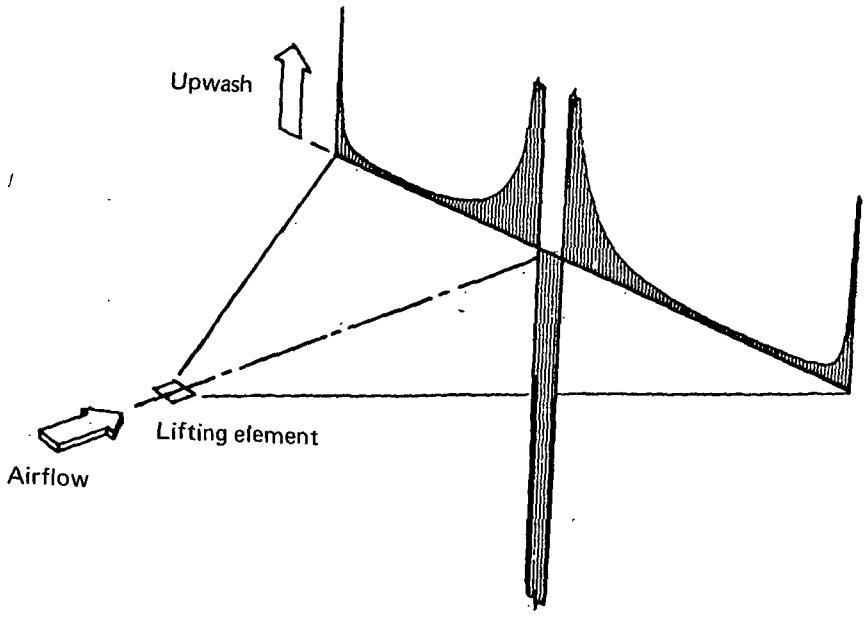

(a) UPWASH PRODUCED BY LIFTING ELEMENT

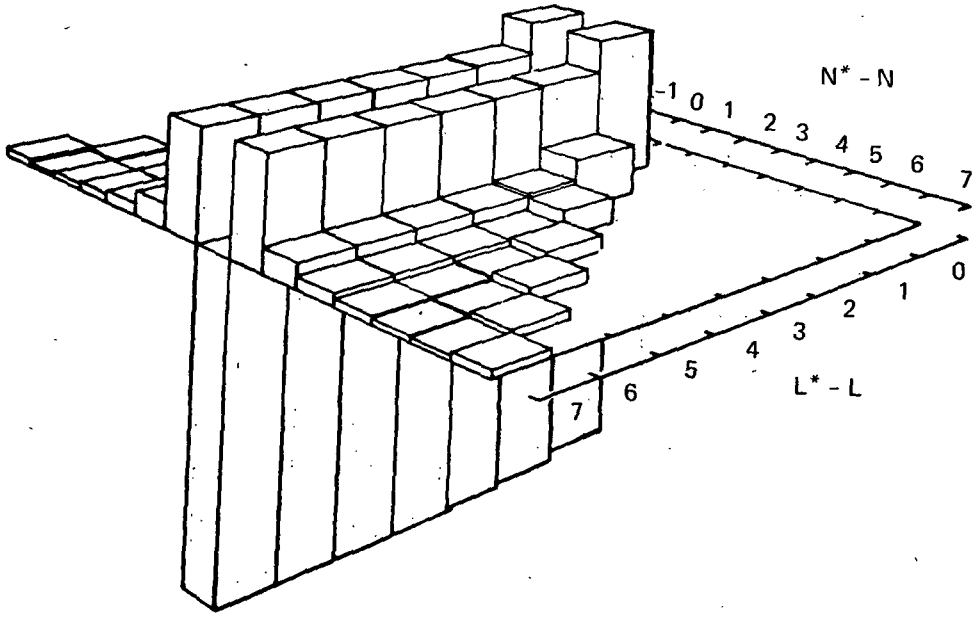

(b) NUMERICAL REPRESENTATION OF $\bar{R}$ FUNCTION

FIGURE 4.4-3.—INFLUENCE FACTOR CHARACTERISTICS

drag-due-to-lift, since a local element may be inclined forward to produce both lift and thrust. Conversely, an element located at the trailing edge and centerline of a diamond planform produces lift inefficiently, since the element sees an influencing region that contributes downwash.

In computing the local surface slope required to obtain a specified lifting pressure coefficient, the ΔCp value is known everywhere on the wing from loading formulas. In the wing design computer program, the wing camber surface shape is found by integrating the surface slopes for all chordwise elements at selected span stations. Section values of drag (ΔCp times slope), lift and pitching moment are then integrated spanwise to obtain wing force coefficients.

Optimum combination of loadings. - Equation 27, which defines the surface slope to support a specified lifting distribution, requires a description of the design pressure distribution. This is obtained from Lagrange's method of undetermined multipliers, which provides a means of selecting an optimum combination of component loadings, yielding minimum drag subject to various imposed constraints on the allowable pressure distribution.

A number of design point options are provided in the wing design program, involving the selection of loadings to be combined and the constraints desired. (The options are controlled by input codes, as described in the user's manual, part 2).

The usual design conditions specified are:

- Drag-due-to-lift of the wing be minimized at a given design lift coefficient, subject to an optional pitching moment constraint.
- Effects of fuselage and nacelles be included in the design solution.
- Constraints be applied to the design pressure distribution to provide physical realism.

The design point options are discussed on page 49.

The optimum loading selection is an extension of the methods used in references 9 and 11, through the addition of the configuration-dependent loadings (due to fuselage and nacelles) and the addition of the pressure constraint formulation. Also, more component loadings were added to provide flexibility in rearranging pressure distributions at the design point in order to meet the pressure

constraint condition. The maximum number of loadings is 17, defined in the table on page 45.

The wing design method actually consists of four solution steps:

- Flat wing solution
- Calculation of aerodynamic characteristics of selected component loadings.
- Optimization of loading combination
- Camber shape calculation

Flat wing solution. - The first step in the wing design process is to obtain the flat wing solution for the given wing planform and Mach number, using the analysis form of the lifting pressure calculation described on page 50. This solution is obtained to locate the wing aerodynamic center for use in computing the pitching moment at zero lift for the individual loadings; and also, because its drag-due-to-lift factor is an often-used reference point in judging twisted and cambered wing designs.

Component loadings characteristics. - For each selected component loading, section lift, drag, and pitching moment coefficients are evaluated at a series of span stations and integrated spanwise to obtain overall lift, drag, and pitching moment. In addition, the interference drag coefficients between loadings are computed, where the drag interference between loadings i and j is given by

$$C_{D,ij} = C_{D,ji} = \frac{1}{\beta S} \sum \Delta C_{p,i}(L^*,N^*)\left(\frac{\partial z}{\partial x}\right)_j (L^*,N^*)\, A(L^*,N^*)\, B(L^*,N^*) \qquad (28)$$

$$+ \frac{1}{\beta S} \sum \Delta C_{p,j}(L^*,N^*)\left(\frac{\partial z}{\partial x}\right)_i (L^*,N^*)\, A(L^*,N^*)\, B(L^*,N^*)$$

where the summations are carried out over the wing planform. For the component loadings defined over the entire planform by analytical expressions, the loading is scaled by the appropriate power of either semispan or average wing chord, so that the resultant component loading lift coefficient is approximately one.

Interference drag coefficients associated with the configuration-dependent loadings are special cases. The configuration-dependent loadings are those produced by fuselage upwash, fuselage volume asymmetry, and nacelles, as described on page 56. They are calculated at discrete points over the wing planform, and

TABLE I

DESCRIPTION OF WING LOADING TERMS

Loading Number	Definition
1.	Uniform
2.	Proportional to x, the distance from the leading edge
3.	Proportional to y, the distance from the wing centerline
4.	Proportional to y^2
5.	Proportional to x^2
6.	Proportional to $x(c - x)$, where c is local chord
7.	Proportional to $x^2 (1.5\, c - x)$
8.	Proportional to $2 (1 + 15 \frac{x}{c})^{-0.5}$
9.	Proportional to $(c - x)^{0.5}$
10.	Elliptical spanwise, proportional to $\sqrt{(1 - y/\frac{b}{2})}$
11.	Proportional to x, the distance from the leading edge of an arbitrarily defined region
12.	A camber-induced loading proportional to the body bouyancy loading
13.	A camber-induced loading proportional to the body upwash loading
14.	A camber-induced loading proportional to the nacelle buoyancy loading
15.	The body bouyancy loading
16.	The body upwash loading
17.	The nacelle buoyancy loading

interpolated linearly for a complete definition where needed . Since there is no camber surface associated with the fuselage loadings, the interference drag coefficient between the "regular" loadings and the configuration dependent loadings has only one term. To ease the computational task of evaluating component and interference characteristics, the configuration-dependent loadings are assigned a corresponding wing slope definition of zero.

The nacelle configuration-dependent loading has yet another difference, since the flow fields of the "regular" loadings act on the fixed geometry of the nacelles, producing an appreciable axial force. The lifting pressure acting on the wing lower surface is assumed to propagate along Mach lines from the wing to the nacelle area distribution, and the associated buoyancy force is computed.

Optimization of loading combination. - Given the aerodynamic characteristics of the component loadings and their interference drag terms, the aerodynamic characteristics of a wing supporting any combination of these component loadings can be calculated in terms of load strength factors A_i assigned to each. The total lift coefficient for n loadings is

$$C_L = \sum_{i=1}^{i=n} C_{L,i} A_i \tag{29}$$

where $C_{L,i}$ denotes the loading and A_i its load strength factor. The total pitching moment coefficient at zero lift is C_{mo}

$$C_{mo} = \sum_{i=1}^{i=n} C_{mo_i} A_i \tag{30}$$

where

$$C_{mo,i} = C_{M,i} - \frac{dC_M}{dC_L} C_{L,i}$$

and the total drag coefficient is

$$C_D = \frac{1}{2} \sum_{i=1}^{i=n} \sum_{j=1}^{j=n} C_{D,i,j} A_i A_j + \sum_{i=1}^{i=n} C_{DWN,i} A_i \tag{31}$$

where the terms $C_{DWN,i}$ are the axial nacelle force coefficients for the component loadings. The contribution of each loading to the lifting pressure coefficient at point j can be summed to give

$$C_{P,j} = \sum_{i=1}^{i=n} C_{P,i,j} \qquad (32)$$

The load strength factors of the configuration-dependent loadings are 1.0, since those loadings are not variable.

Hence, from the component loadings data, the drag, lift, and pitching moment characteristics of an infinite number of wing designs may be immediately calculated in terms of the A_i factors. The formal optimization of the wing loading involves the specification of the set of $A_{i's}$ which gives least drag subject to the imposed constraints.

According to the Lagrangian method, the solution for the optimum A_i values involves the system of linear equations shown in figure 4.4-4, where matrix notation is used for compactness. The term $*C_{p,i}$ is the allowable lifting pressure coefficient corresponding to the i th pressure limiting constraint on the wing upper surface pressure.

Partitions in the square matrix of the solution have been identified by number and letter in figure 4.4-4. The left, uppermost partition of this matrix (zone A1) and the adjacent row and column correspond to Grant's original design solution (reference 14). The next m rows (zones C1-C5) and columns (zones A3-E3) are introduced by m local constraints on the lifting pressure coefficient, which are added (if necessary) in applying the pressure limiting constraint, as described on page 49.

The next three rows (zones D1-D5) and columns (A4-E4) correspond to the constraints which set the loading factors A_i to 1.0 for the body bouyancy, body upwash, and nacelle buoyancy loadings. Each of these three rows and columns is present only if the corresponding configuration dependent loading is used. The right-hand column (zones A5-E5) and bottom row (zones E1-E5) correspond to the constraint on pitching moment coefficient at zero lift; this constraint is also optional.

The unknowns of the design solution are the n values of the loading factors A_i and the (m+5) Lagrange multipliers (λ_i). These are contained in the left-hand-side column matrix.

	①			②	③			④			⑤		
	$C_{D,11}$	$C_{D,12}$	$C_{D,1N}$	$C_{L,1}$	$C_{p,11}$	$C_{p,12}$	$C_{p,1M}$	0	0	0	$C_{mo,1}$	A_2	$-C_{DWN,1}$
Ⓐ	$C_{D,21}$	$C_{D,22}$	$C_{D,2N}$	$C_{L,2}$	$C_{p,21}$	$C_{p,22}$	$C_{p,2M}$	0	0	0	$C_{mo,2}$	A_1	$-C_{DWN,2}$
								0	0	1.0			
								0	1.0	0			
	$C_{D,N1}$	$C_{D,N2}$	$C_{D,NN}$	$C_{L,N}$	$C_{p,N1}$	$C_{p,N2}$	$C_{p,NM}$	1.0	0	0	$C_{mo,2}$		$-C_{DWN,N}$
Ⓑ	$C_{L,1}$	$C_{L,2}$	$C_{L,N}$	0	0	0	0	0	0	0	0	λ_1	C_L
	$C_{p,11}$	$C_{p,21}$	$C_{p,N1}$	0	0	0	0	0	0	0	0	λ_2	$*C_{p,1}$
	$C_{p,12}$	$C_{p,22}$	$C_{p,N2}$	0	0	0	0	0	0	0	0	λ_3	$*C_{p,2}$
Ⓒ													
	$C_{p,1M}$	$C_{p,2M}$	$C_{p,NM}$	0	0	0	0	0	0	0	0	λ_{M+1}	$*C_{p,M}$
	0	0	0 1.0	0	0	0	0	0	0	0	0	λ_{M+2}	1.0
Ⓓ	0	0	0 1.0 0	0	0	0	0	0	0	0	0	λ_{M+3}	1.0
	0	0	1.0 0 0	0	0	0	0	0	0	0	0	λ_{M+4}	1.0
Ⓔ	$C_{mo,1}$	$C_{mo,2}$	$C_{mo,N}$	0	0	0	0	0	0	0	0	λ_{M+5}	C_{mo}

N number of component loadings
M = number of constraints on wing lifting pressure
All pressure coefficients in figure are lifting pressure coefficients

FIGURE 4.4-4.—OPTIMIZATION MATRIX

The five partitions of the right-hand-side column matrix contain: either the negative of the nacelle interference drag produced by wing lift, or zero if nacelles are not used; the design lift coefficient; the constraint values applied to the lifting pressure coefficient (these are generated automatically by the design computer program, if they are necessary); the values of A_i for the three configuration-dependent loadings; and the design pitching moment coefficient at zero lift.

The maximum number of equations in figure 4.4-4 is 34. This number of equations can be reached if 17 loadings are combined, a pitching moment constraint is used, and the maximum number of constraints on lifting pressure coefficient are required.

Design camber surface. - Given the set of A_i factors, the design pressure distribution is known and the resulting camber surface is calculated using equation 27 on page 40.

Design point options. - Due to options in the wing design program to limit the solution extent (e.g., no C_{m_o} constraint or no pressure limiting constraint), some parts of the solution matrix on page 48 may not be used. However, for purposes of describing the solution options, it is assumed that all options are chosen. In that case, the wing loading solution proceeds as follows, using repeated applications of the corresponding matrix:

(1) The wing loading having minimum lift-dependent drag with a constraint on design lift coefficient only, is defined.

(2) A family of wing loadings having minimum lift-dependent drag with a constraint on design lift coefficient and a series of constraints on pitching moment coefficient at zero lift are defined. This series of solutions is presented in the form of drag due to lift factor, K_E, versus C_{m_o}, and is referred to as the "bucket" plot.

(3) The wing loading having minimum lift-dependent drag with constraints on design lift coefficient and wing upper surface pressure is found. This solution may require a cyclic process for the pressure constraints that begins with (1) above. If (1) satisfies the pressure limits everywhere, then this loading is set equal to (1). If (1) does not satisfy the pressure limits everywhere, then a pressure constraint is applied at the wing planform location where the pressure limit is

most strongly violated, and a new solution for wing loading is found. Its pressure distribution is tested against the limit, and another constraint is imposed if the limit is violated. Each cycle adds another pressure constraint to the solution in addition to the lift coefficient constraint. Cycling stops either when a solution load distribution everywhere satisfies the pressure limit or when the number of solution constraints is equal to the number of loadings.

(4) The wing loading having minimum lift-dependent drag with constraints on design lift coefficient and zero-lift pitching moment coefficient is defined.

(5) The wing loading having minimum lift-dependent drag with constraints on design lift coefficient, pitching moment coefficient at zero lift, and wing upper surface pressure is found. The latter type of constraints are imposed, if necessary, in the cyclic fashion of (3).

Examples of loading solutions (1), (2), (4), and (5) are shown in figure 4.4-5. For this case, loading solution (1) satisfies the wing upper surface pressure constraint, and is therefore identical to loading solution (3).

The effect of the number of loadings on the "bucket" plot and on loading solution (5) is illustrated in figure 4.4-6. Increasing the number of loadings from 3 to 7 results in a substantial theoretical drag decrease, much greater than the reduction obtained in further increase of loadings to 10.

A discussion of the loading selection and the resultant camber surface optimization is presented in part 2 (user's manual).

Lift Analysis Case

Loading for a given camber surface. - Since the $\bar{R}$ function for the field point element is zero (the element generates no downwash or upwash upon itself), equation 27 can be rearranged to solve for the lifting pressure coefficient in terms of the field point slope and upstream influences:

$$\Delta C_p\,(L^*,N^*) = -\frac{4}{\beta}\frac{dz_c}{dx}\,(L^*,N^*) + \frac{1}{\pi}\sum_{\tau}\bar{R}(L^*-L,N^*-N)\,A(L,N)\,B(L,N)\,C(L,N)\,\Delta C_p(L,N) \tag{33}$$

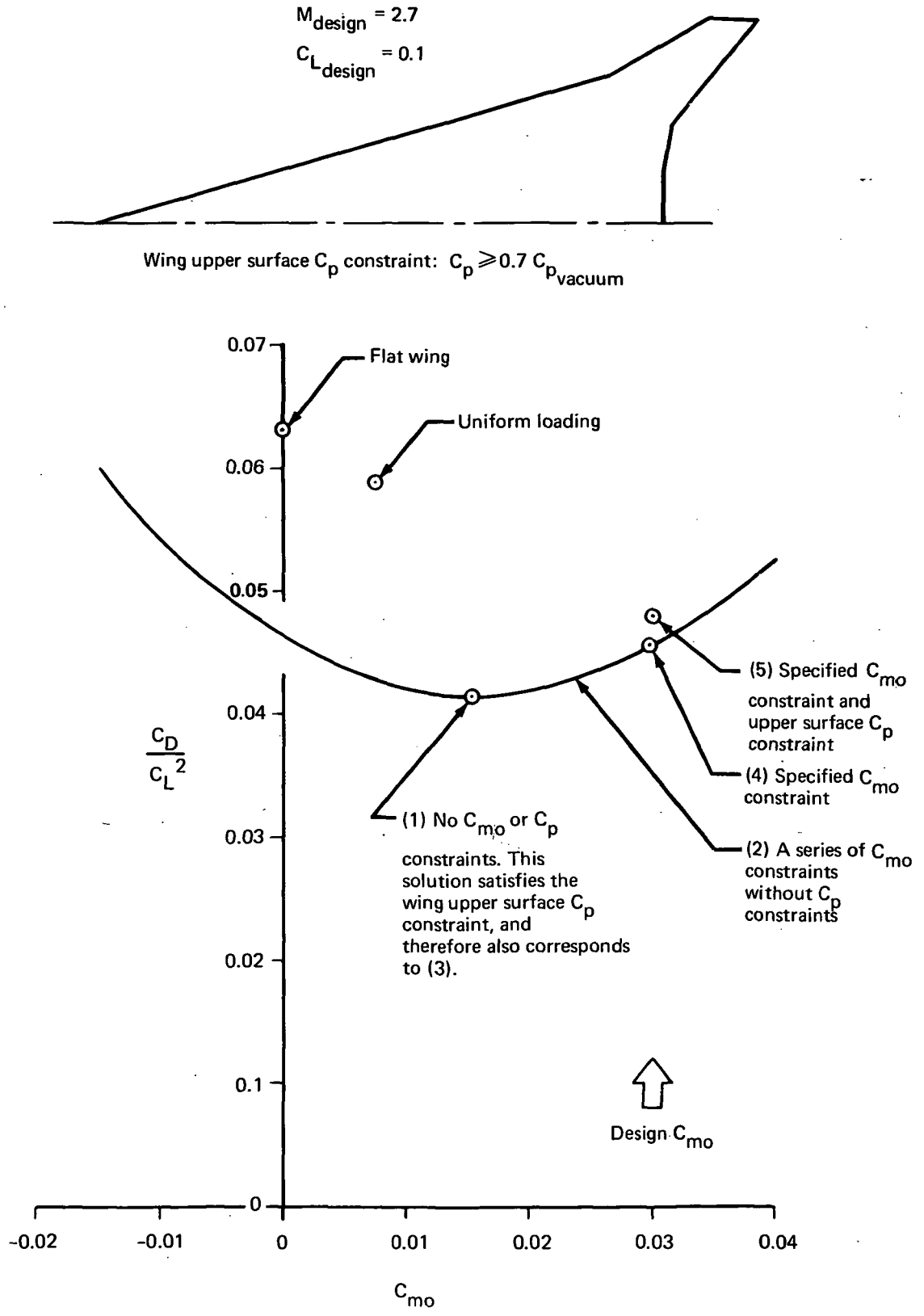

FIGURE 4.4-5.—TYPES OF LOADING SOLUTIONS

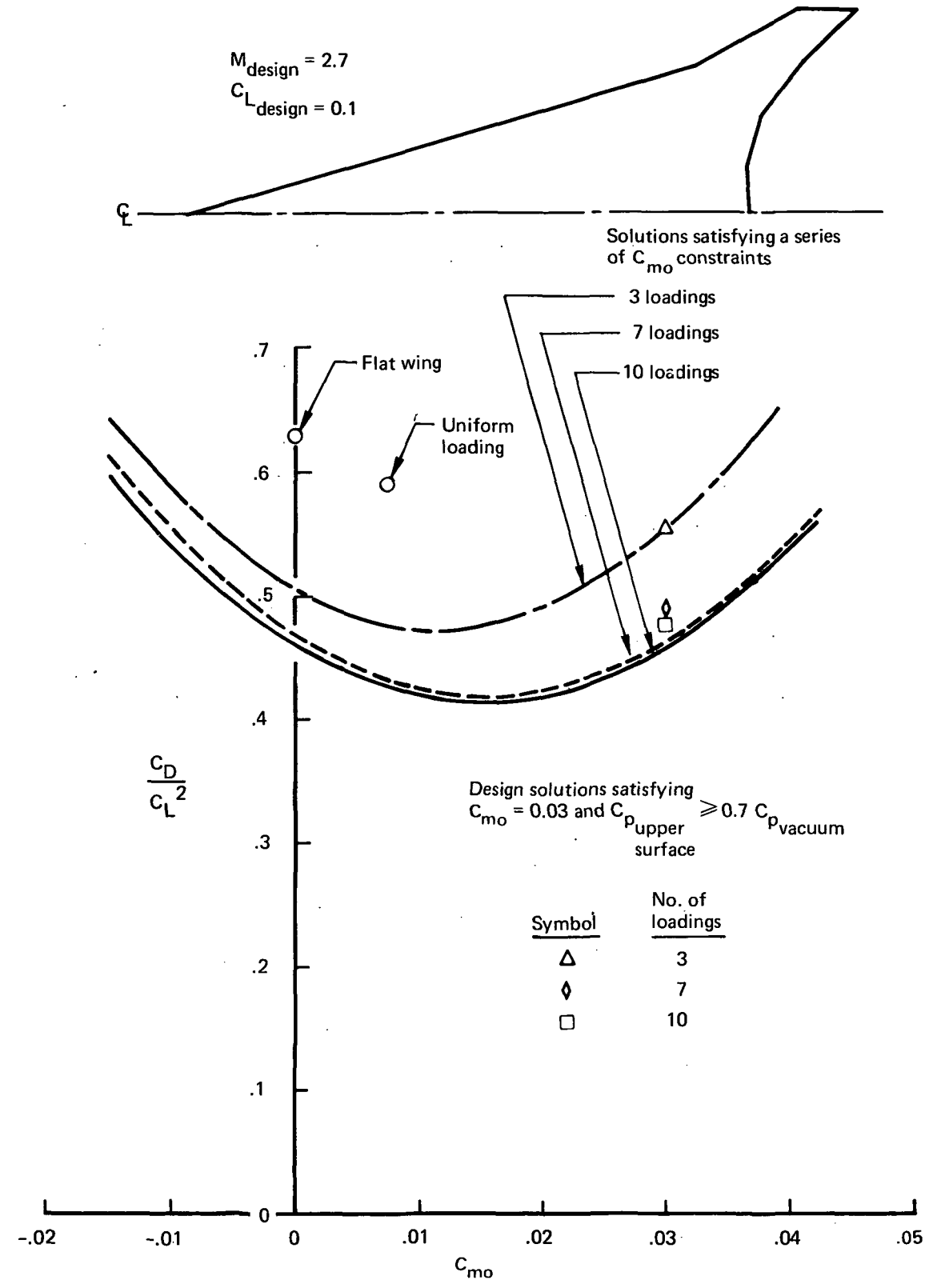

FIGURE 4.4-6.—THEORETICAL EFFECT OF NUMBER OF LOADINGS ON DESIGN SOLUTION

Therefore, the lifting pressure distribution, ΔCp, can be determined for a wing of arbitrary surface shape provided the calculations are performed in the proper sequence. The order of calculation of $\Delta Cp(L^*,N^*)$ is from apex aft, and from the centerline to the right hand wing tip for each L^* row. In this fashion, all pressure coefficients within the Mach forecone from any element will have been previously obtained and no unknown pressure coefficients arise in the summation. The element fractions A, B, and C are as defined for equation 27.

Theoretically, $\Delta Cp(L^*, N^*)$ defined by equation 33 is the pressure coefficient at the aft mid-point of the L^*, N^* element. The average pressure coefficient for the element, needed in subsequent calculations, is calculated by one of two alternative methods:

1) An approximate average pressure coefficient is interpolated from the aft mid-point ΔCp value and the ΔCp value of the element immediately ahead. (No interpolation is performed if L^*, N^* is a leading edge element). This is the method used in the original formulation of the computer program. However, it was found that osillations in the ΔCp values occurred near the wing leading edge. So, a 9 point smoothing equation was applied after unsmoothed pressures were computed for the entire wing, which essentially removed the oscillations and brought the smoothed pressure distribution into good agreement with established results from other theoretical methods. The smoothing equation is of the form

(34)

$$\overline{\Delta C_p}(L^*) = \frac{\begin{aligned}&0.2A(L^*-4)\Delta C_p(L^*-4) + 0.4A(L^*-3)\Delta C_p(L^*-3) + 0.6A(L^*-2)\Delta C_p(L^*-2)\\&+ 0.8A(L^*-1)\Delta C_p(L^*-1) + A(L^*)\Delta C_p(L^*) + 0.8A(L^*+1)\Delta C_p(L^*+1)\\&+ 0.6A(L^*+2)\Delta C_p(L^*+2) + 0.4A(L^*+3)\Delta C_p(L^*+3) + 0.2A(L^*+4)\Delta C_p(L^*+4)\end{aligned}}{\begin{aligned}&0.2A(L^*-4) + 0.4A(L^*-3) + 0.6A(L^*-2) + 0.8A(L^*-1) + A(L^*) + 0.8A(L^*+1)\\&+ 0.6A(L^*+2) + 0.4A(L^*+3) + 0.2A(L^*+4)\end{aligned}}$$

where the A values account for element fractions. A is zero if the corresponding element is ahead of the wing leading edge, or aft of trailing edge in the case of a subsonic trailing edge. The supersonic trailing edge solution is treated as a special case, and the trailing edge is extended four elements to provide pressure coefficient data to fill out the smoothing equation.

2) The other average ΔCp method is an improved technique, which uses an aft element sensing approach. This method involves solving for preliminary ΔCp results for a given L^*, N^* element and the element immediately aft, then

following it up with a second calculation to refine the preliminary results. The procedure is detailed in reference 12, but is summarized below and in figure 4.4-7.

a) Calculate preliminary ΔCp values for a given L* = constant row. Designate as $\Delta C_{p,a}(L^*,N^*)$

b) Calculate preliminary ΔCp values for the element row immediately aft = L*+1, using $\Delta C_{p,a}$ values. Designate as $\Delta C_{p,b}(L^*,N^*)$.

c) Finalize Cp values for the original L* = constant row from one of the two following equations.
For leading edge elements:

$$\Delta C_p(L^*,N^*) = \frac{1}{2}\left[1 + \frac{A(L^*,N^*)}{1 + A(L^*,N^*)}\right]\Delta C_{p,a}(L^*,N^*) + \frac{1}{2}\left[\frac{A(L^*,N^*)}{1 + A(L^*,N^*)}\right]\Delta C_{p,b}(L^*,N^*) \quad (35)$$

For all other elements:

$$\Delta C_p = \frac{3}{4}\Delta C_{p,a}(L^*,N^*) + \frac{1}{4}\Delta C_{p,b}(L^*,N^*) \quad (36)$$

The aft element sensing technique produces a substantial reduction in pressure coefficient oscillation. In cambered wing test cases run with the method, however, some oscillation was found to persist. Therefore, a 3 term smoothing equation was added (after all wing pressures are calculated), of the form:

$$\overline{\Delta C}_p(L^*) = \frac{0.5A(L^*-1)\Delta C_p(L^*-1) + \Delta C_p(L^*) + 0.5A(L^*+1)\Delta C_p(L^*+1)}{0.5A(L^*-1) + 1.0 + 0.5A(L^*+1)} \quad (37)$$

In the computer program one of the two alternate smoothing methods is selected by an input code. Both produce essentially the same answers . When the pressure limiting option is used (discussed later), the aft-sensing smoothing technique is automatically selected.

For the analysis solution, the pressure coefficients for all elements must be calculated. The force coefficients are, therefore, calculated from direct summations of local pressures applied to each element, rather than employing a spanwise integration as in the design case. Lengthwise and spanwise lift distributions are obtained by summing the lift in the corresponding element rows.

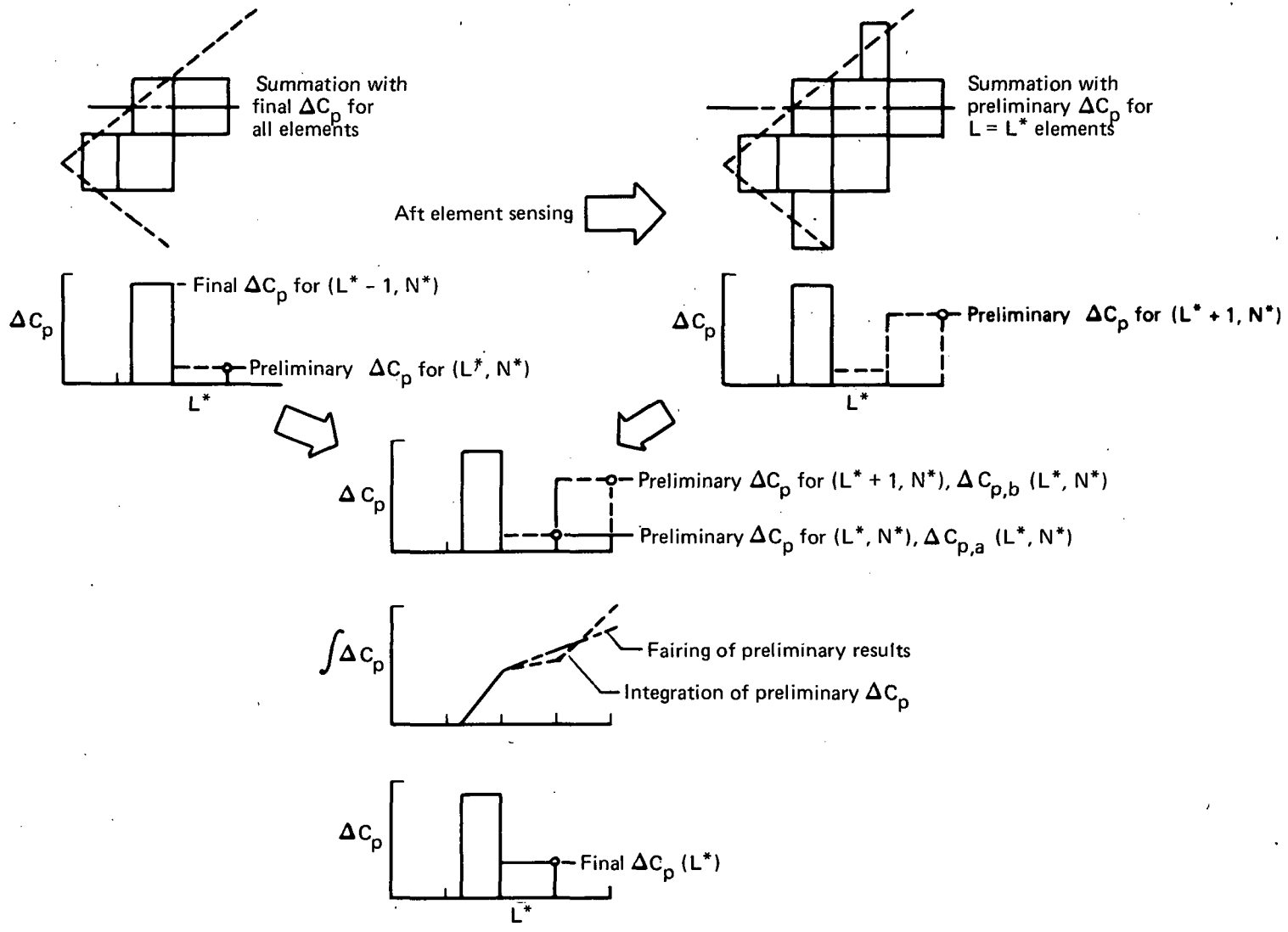

FIGURE 4.4-7.—APPLICATION OF AFT-ELEMENT SMOOTHING TECHNIQUE (FROM REF. 12)

No "leading-edge-suction" force is included in the drag summation, which accounts only for the lifting pressure coefficients acting on the local wing slopes.

Analysis of complete configuration. - preceding discussion describes the theory used in the lifting pressure calculations for a wing camber surface at a selected angle of attack. The analysis program may also be used to calculate lifting pressure distributions and force coefficients for complete configurations over a range of angles of attack, adding in the effects of fuselage, nacelle, canard and/or horizontal tail, as applicable.

The program actually carries two solutions along: one for the configuration at its input angle of attack, the other the incremental solution per degree angle of attack (called the flat wing solution). The interference terms associated with the two solutions acting on the other surface shape are also calculated. The summation of these effects into the drag polar and other force coefficients is performed by superposition, as described on page 64.

Calculation of the complete configuration lifting pressure solution involves up to 7 principal tasks:

- Isolated fuselage upwash field
- Nacelle pressure field acting on wing
- Pressure field due to asymmetrical fuselage volume
- Wing/canard solution in presence of fuselage upwash field. Effects of the wing pressure field acting on nacelles, are also calculated
- Fuselage lift distribution in presence of wing downwash field
- Horizontal tail solution in presence of fuselage and wing flow fields.
- Superposition of solutions

The calculation logic of these tasks is described in the following sections:

Isolated fuselage upwash field. - The fuselage upwash (or downwash) field in the plane of the wing, canard or horizontal tail is obtained from slender body theory. From reference 15, the velocity potential of a slender body of revolution, shown in figure 4.4-8, is:

$$\frac{1}{U}\phi(x,r,\theta) = \frac{1}{2\pi}\frac{dA(x)}{dx}\ell n\frac{\beta r}{2} - \frac{1}{2\pi}\frac{\partial}{\partial x}\int_0^x \frac{dA(x)}{dx}\ell n(x-x_1)dx_1 + [\alpha+\varepsilon(x)]R^2(x)\frac{\cos\theta}{r} \qquad (38)$$

The nondimensional radial velocity component is

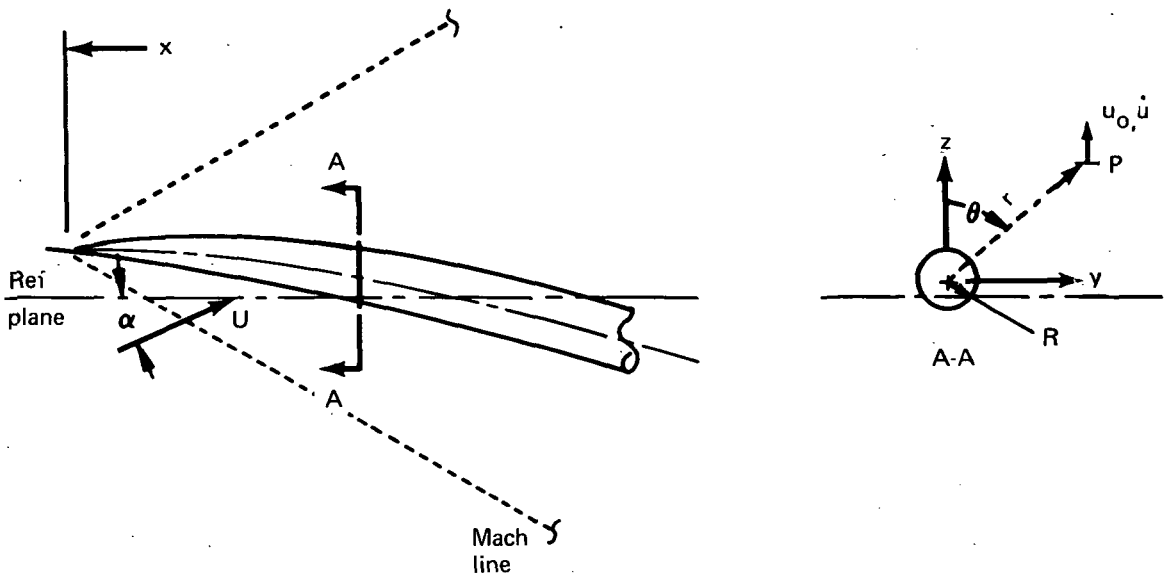

Upwash propagates along Mach lines.
Upwash at arbitrary point P is:

$$\frac{w_o}{U} = u_o = \frac{1}{2\pi}\frac{dA(x)}{dx}\frac{z}{r^2} - \epsilon(x)\frac{R^2(x)}{r^2}\left(\frac{z^2-y^2}{r^2}\right)$$

$$\frac{\dot{w}}{U} = \dot{u} = -\frac{R^2(x)}{r^2}\left(\frac{z^2-y^2}{r^2}\right)$$

Where:

u_o = upwash at input fuselage incidence ($\alpha = 0$)

$\dot{u}$ = upwash increment per unit α

A(x), R(x) = Fuselage cross-sectional area, radius

$\epsilon(x)$ = Fuselage incidence due to camber (relative to reference plane)

z,y,r = location of point at which upwash is calculated

α = angle of attack of reference plane

U = free stream velocity

FIGURE 4.4-8.–FUSELAGE UPWASH CALCULATION

$$\frac{1}{U}\phi_r = \frac{1}{2\pi r}\frac{dA(x)}{dx} - \frac{\alpha + \varepsilon(x)}{r^2} R^2(x) \cos\theta \qquad (39)$$

and the tangential component is

$$\frac{1}{Ur}\phi_\theta = -[\alpha + \varepsilon(x)]\frac{R^2(x)}{r^2}\sin\theta \qquad (40)$$

The vertical velocity component (upwash angle) is

$$\frac{w}{U} = \frac{1}{U}\phi_r \cos\theta - \frac{1}{Ur}\phi_\theta \sin\theta \qquad (41)$$

Substituting for ϕ_r and ϕ_θ and converting to cartesian coordinates gives

$$\frac{w}{U} = \frac{1}{2\pi}\frac{dA(x)}{dx}\frac{z}{r^2} - [\alpha + \varepsilon(x)]\frac{R^2(x)}{r^2}\left(\frac{z^2 - y^2}{r^2}\right) \qquad (42)$$

When the fuselage is at input incidence, the fuselage upwash is

$$u_o = \frac{1}{2\pi}\frac{dA(x)}{dx}\frac{z}{r^2} - \varepsilon(x)\frac{R^2(x)}{r^2}\left(\frac{z^2 - y^2}{r^2}\right) \qquad (43)$$

and the incremental upwash per degree angle of attack increase is

$$\dot{u} = \frac{d\, w/u}{d\alpha} = -\frac{R^2(x)}{r^2}\left(\frac{z^2 - y^2}{r^2}\right) \qquad (44)$$

Slender body theory assumes that the upwash field propagates normal to the body centerline. In the analysis program, the fuselage upwash is propagated along Mach lines, as required by the characteristics of supersonic flow.

Nacelle pressure field acting on wing. - The pressure field caused by the nacelles on the wing is calculated by the Whitham solution, as described in Section 4.3. The nacelles are assumed to be bodies of revolution, and the pressure signature due to each nacelle is calculated for a series of spanwise stations from wing root to tip. The composite pressure signature at a given spanwise station is the sum of the individual nacelle signatures, with all pressure coefficients doubled to account for reflection from the wing. Either "wrap" or "glance" nacelles may be used, as discussed in Section 4.3.

Pressure field due to asymmetric fuselage volume. - Another term in the superposition approach is associated with the growth in fuselage area above and below the wing. If the area growth is

asymmetric (e.g., a low wing configuration), a differential pressure across the wing plane is created which is additive to the effect created by the fuselage upwash field.

An approximate method of computing the asymmetric fuselage pressure field is used, using the area distributions shown in figure 4.4-9. To the actual forebody area distribution is added the growth in fuselage area in the wing region relative to the area at the leading edge of the wing-fuselage intersection. This is done for both the below- amd above-wing area distributions. Pressure signatures for both body representations are computed using the Whitham technique at a series of spanwise stations, doubled to account for reflection from the wing, and differenced to get the lifting pressure distribution due to asymmetric fuselage volume.

If the wing trailing edge is subsonic, the pressure fields above or below the wing revert to that corresponding to the actual fuselage area distribution in the region aft of a Mach line from the trailing edge of the wing-fuselage intersection.

Use of the asymmetric fuselage calculation is controlled by an input code in the computer program. If the asymmetric calculation is not requested, the fuselage pressure field corresponding to a mid-wing arrangement is calculated, so that there will always be a thickness pressure field due to the fuselage, if present, for use in limiting pressure calculations (discussed later).

Wing/Canard Solution in Presence of Fuselage and Nacelles

The wing or canard lifting pressure solution in the presence of fuselage and/or nacelles is performed as described for the isolated wing, with the following alterations:

- The local surface angles of attack are increased by the fuselage upwash values for the purposes of computing pressure coefficients. (To compute drag, the pressure coefficient is applied to the local surface slopes, only).

- In the region of the wing covered by the fuselage, the wing slopes are zeroed. This reflects the fact that the wing lift distribution in this region is of the "carry-over" type, only. (To compute drag, the carry-over lift is applied to the fuselage camber line shape)

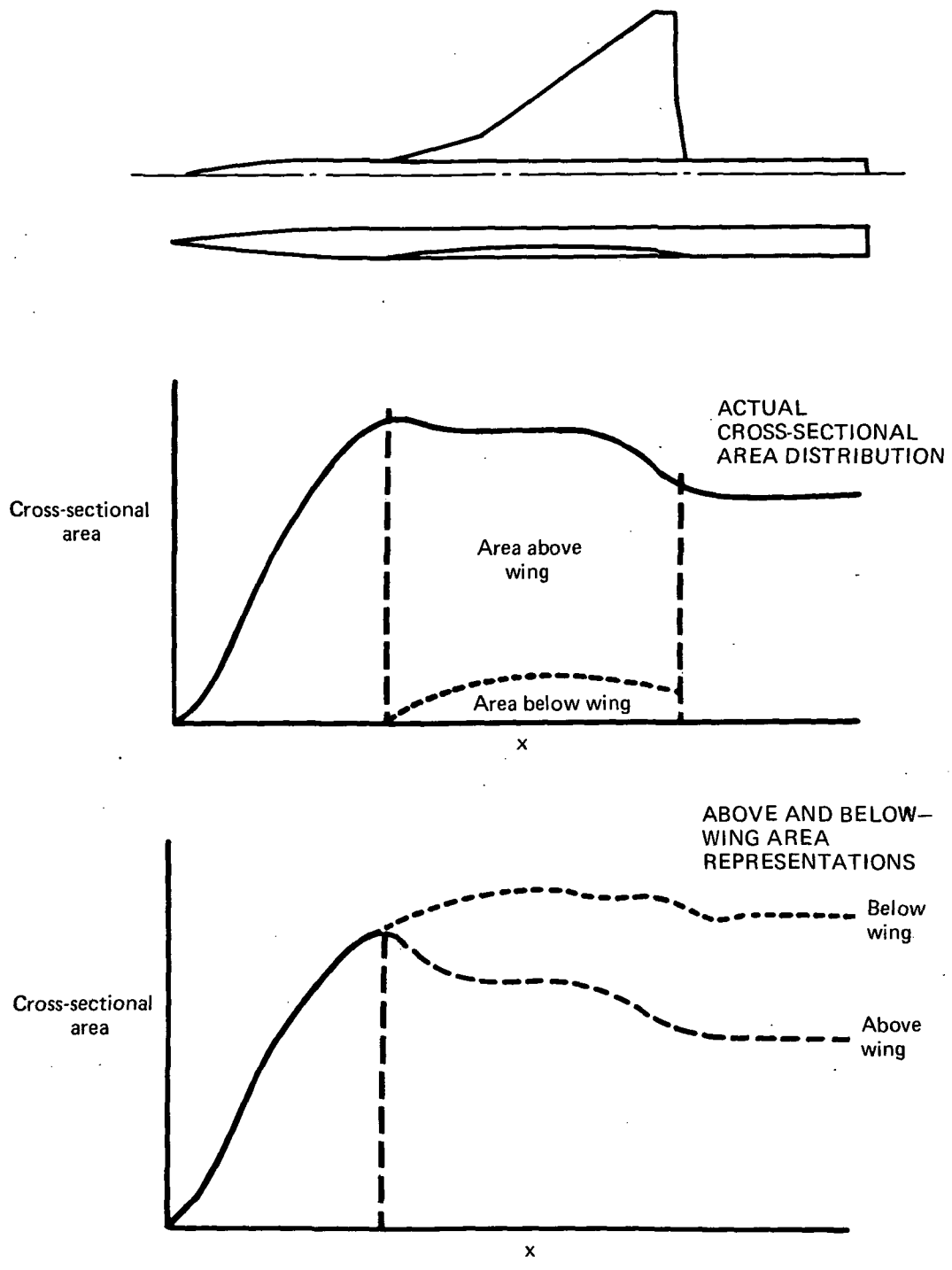

FIGURE 4.4-9.– FUSELAGE AREA REPRESENTATION FOR ASYMMETRIC FUSELAGE BUOYANCY FIELD

- The canard pressure distributions are computed in the same fashion as the wing pressure distribution, with the canard also creating a downwash (or upwash) field for the wing.

The nacelle or asymmetric fuselage volume pressure fields are superimposed upon the wing elements to obtain the effect of the nacelles or fuselage asymmetry on the wing. If nacelles are present, the buoyancy drag of the wing lifting pressures acting on the nacelle area distribution is also calculated. This term is obtained by transferring local wing pressures aft along Mach lines to act upon the nacelle area growth, in a fashion paralleling the wing-thickness-on-nacelle term of the near-field wave drag program.

Fuselage lift distribution in presence of wing downwash field. - From slender body theory , the fuselage lift distribution is given by

$$c_\ell \cdot R(x) = \frac{dA(x)}{dx} [\alpha + \varepsilon(x)] + \frac{d}{dx} [\varepsilon(x) \cdot A(x)] \qquad (45)$$

using the notation of figure 4.4-8.

The first term of the equation is the slender body term associated with a straight body at angle of attack; the second term is due to the curvature change associated with body camber.

In computing the fuselage lift distribution, the downwash (or upwash) from the wing/canard is included in the local angle of attack term, ϵ . For drag computations, the lift is applied only to the physical angle of attack value, $\alpha + \epsilon(x)$.

Fuselage force coefficients (lift, drag, and pitching moment) are calculated from the slender body lift distribution and converted to a wing reference area basis for summation into the complete configuration characteristics.

Horizontal tail solution. - The horizontal tail lifting pressure distribution is calculated in the presence of the fuselage upwash field and wing/canard downwash field. The solution employs the same logic of partitioning the tail into exposed and carry-over regions used in the wing and canard pressure computations.

Since the horizontal tail is assumed to be aft of the wing, the fuselage and wing/canard upwash (or downwash) field is first calculated, then the tail lift distribution and force coefficients are computed for the desired tail angles of attack. These are summed into the wing/fuselage, etc., solution for each tail angle, resulting in a set of force coefficients for each tail setting in the same fashion as wind tunnel data are obtained.

Calculation of the wing/canard downwash field is performed by extending the wing grid system aft to include the horizontal tail. With all pressure coefficients on the wing or canard previously established, the effect of the wing/canard on the horizontal tail is obtained from

$$\Delta_{W,C} = \sum_{\tau}^{Wing} \bar{R}\,(L^* - L,\ N^* - N)\ A\,(L,\ N)\ B(L,\ N)\ C(L,\ N)\ \Delta C_p\,(L,\ N)$$
$$+ \sum_{\tau}^{Canard} \bar{R}\,(L^* - L,\ N^* - N)\ A(L,\ N)\ B(L,\ N)\ C(L,\ N)\ \Delta C_p\,(L,\ N) \qquad (46)$$

in which the wing, canard, and tail are all assumed to be located in essentially the same plane.

Calculation of the horizontal tail lifting pressures are then performed using the analysis form of the lifting pressure equation

$$\Delta C_p\,(L^*,\ N^*) = -\frac{4}{\beta}\frac{dz}{dx}\,(L^*,\ N^*)$$
$$+ \frac{1}{\pi}\sum_{\tau}^{Tail} \bar{R}\,(L^* - L,\ N^* - N)\ A(L,\ N)\ B(L,\ N)\ C(L,\ N)\ \Delta C_p\,(L,\ N) + \Delta_{W,C} \qquad (47)$$

with the wing/canard term added to the summation of upstream effects. As in the wing/canard pressure solution, the fuselage upwash is added to the physical tail slope for the purposes of computing lifting pressures, but removed for the calculation of the drag term. The carry-over lift of the horizontal tail is applied to the fuselage camber line to obtain the drag interference of the tail on the fuselage.

The effect of wing downwash on the horizontal tail lifting pressures is significant. The data of figure 4.4-10 show the theoretical drag and pitching moment increments at constant total lift for a typical configuration, with and without wing downwash included. (Comparisons of the theoretical calculations with experimental data are presented in the user's manual, part 2.)

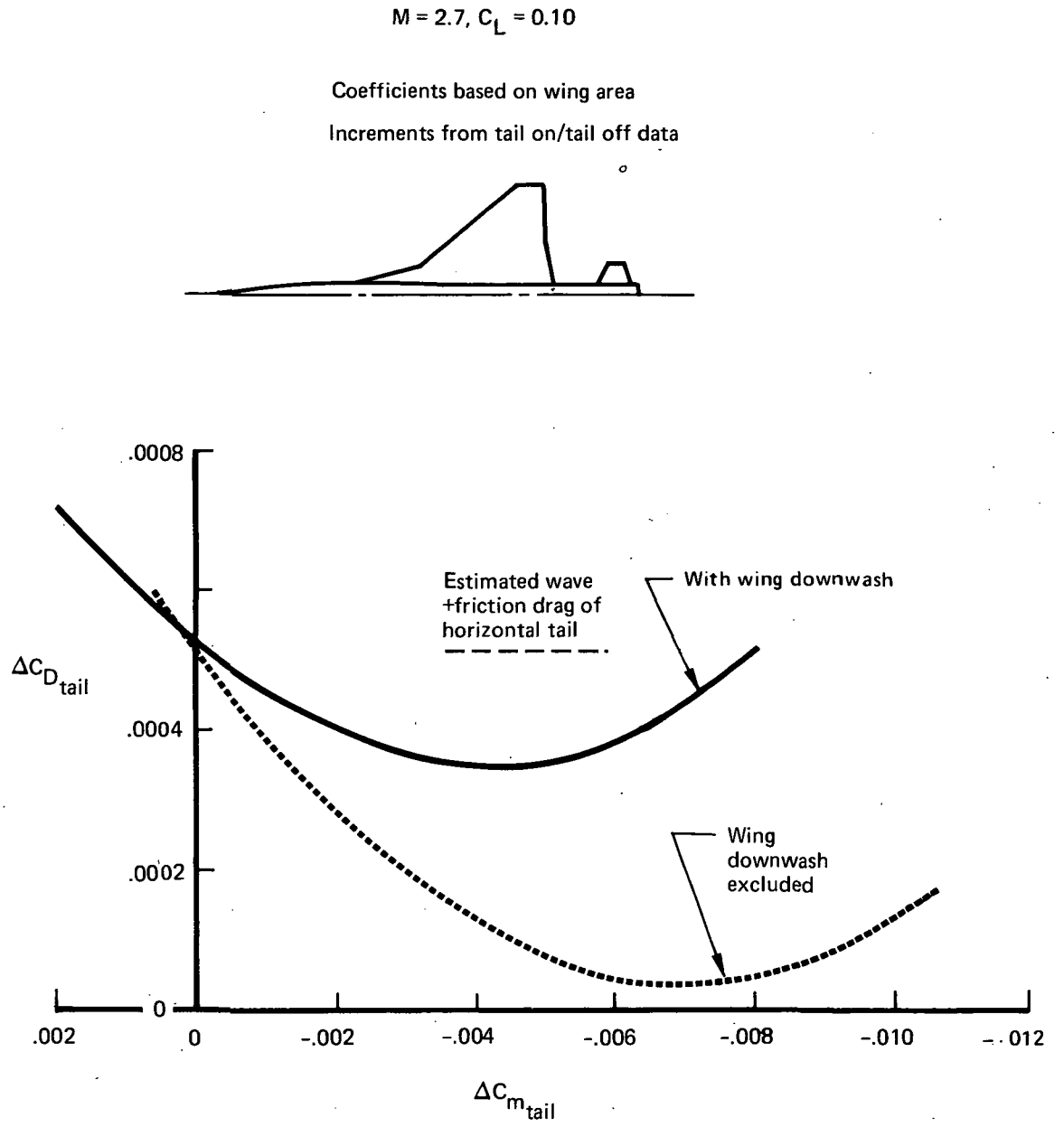

FIGURE 4.4-10.—EFFECT OF WING DOWNWASH ON TAIL (THEORETICAL ESTIMATE)

Superposition of Solutions

The arrangement of terms in the superposition of the complete configuration force coefficients is:

$$C_L = \Sigma C_{L_{\alpha = 0}} + \alpha \Sigma \Delta C_L \tag{48}$$

$$C_m = \Sigma C_{m_{\alpha = 0}} + \alpha \Sigma \Delta C_m \tag{49}$$

$$C_D = \Sigma C_{D_{\alpha = 0}} + K_1 (C_L - C_{L_{\alpha = 0}}) + K_2 (C_L - C_{L_{\alpha = 0}})^2 \tag{50}$$

where the lift, drag, and pitching moment coefficients at $\alpha = 0$ correspond to the individual fuselage, wing, tail, etc., solutions at input configuration incidence, and the ΔC_L and ΔC_m coefficients correspond to the incremental (flat wing) solutions per degree angle of attack.

The drag coefficient equation includes the interference terms between the solution at input incidence and the incremental solution per degree. With subscripts C and F denoting input incidence and the flat wing terms, respectively, the drag coefficient equation is:

$$C_D = C_{D_C} + (C_{D_{FOC}} + C_{D_{COF}}) \frac{\alpha}{\alpha_F} + \frac{\alpha}{\alpha_F} C_{L_F} \alpha \tag{51}$$

$$\text{or } C_D = C_{D_C} + \frac{(C_{D_{FOC}} + C_{D_{COF}})}{C_{L_F}} (C_L - C_{L_C}) + \frac{0.01745 (C_L - C_{L_C})^2}{C_{L_F}} \tag{52}$$

where α = configuration angle of attack

α_F = flat wing incidence, .01745 radian

$$C_{L_C} = \frac{1}{S} \Sigma \Delta C_{p_C} A_E \qquad C_{D_C} = \frac{1}{S} \Sigma \Delta C_{p_c} A_E \alpha_C$$

$$C_{L_F} = \frac{1}{S} \Sigma \Delta C_{p_F} A_E \qquad C_{D_F} = \alpha_F C_{L_F}$$

with A_E = local element area corresponding to ΔC_{p_C}

S = reference area

α_C = local element slope

$C_{D_{FOC}} = \frac{1}{S} \sum \Delta C_{p_F} A_E \alpha_C$ — interference drag of flat wing pressures acting on cambered wing slopes, per degree.

$C_{D_{COF}} = \alpha_F C_{L_C}$ — interference drag of cambered wing pressures acting on flat wing incidence, per degree.

with the summations carried out over the wing planform.

Therefore, for each of the solutions involved in the superposition, it is necessary to calculate both an input incidence solution, a flat wing solution, and the interference drag terms between the two solutions. All of the force coefficients are referred to an input area, moment center, and moment reference length in the summations.

Limiting pressure solution. - Linear theory imposes no restrictions on the allowable wing pressure coefficients. Particularly in the case of subsonic leading edge wings, large upper surface pressure coefficients may be computed near the outboard wing leading edge that exceed (are more negative than) pressure coefficients corresponding to a vacuum. These pressure coefficients can occur at moderate wing angles of attack, due to the strength of the upwash generated by the inboard wing.

Several investigators have examined experimental data to define the minimum attainable upper surface pressure coefficients. One such correlation is shown in figure 4.4-11 (from reference 16), which indicates a physical pressure coefficient limit of approximately .8 vacuum. The mechanism of this limiting is associated with local leading edge flow separation. However, the phenomenon may be approximated in the wing analysis program by limiting the calculated linear theory pressure coefficients to a specified fraction of vacuum C_p.

In the analysis program, pressure limiting is an optional feature, controlled by an input code. If limiting is requested, then a set of configuration angles of attack is required for the solution, since superposition will not apply after limiting occurs. Also, a definition of the wing thickness pressures is required (transferred over from the near field wave drag program module), since it is the sum of lifting plus thickness pressures that is limited, rather than the lifting pressure alone.

Pressure coefficients, as calculated, are separated into upper and lower surface values. Thickness pressures (wing plus fuselage) are added and the upper surface pressure coefficient tested

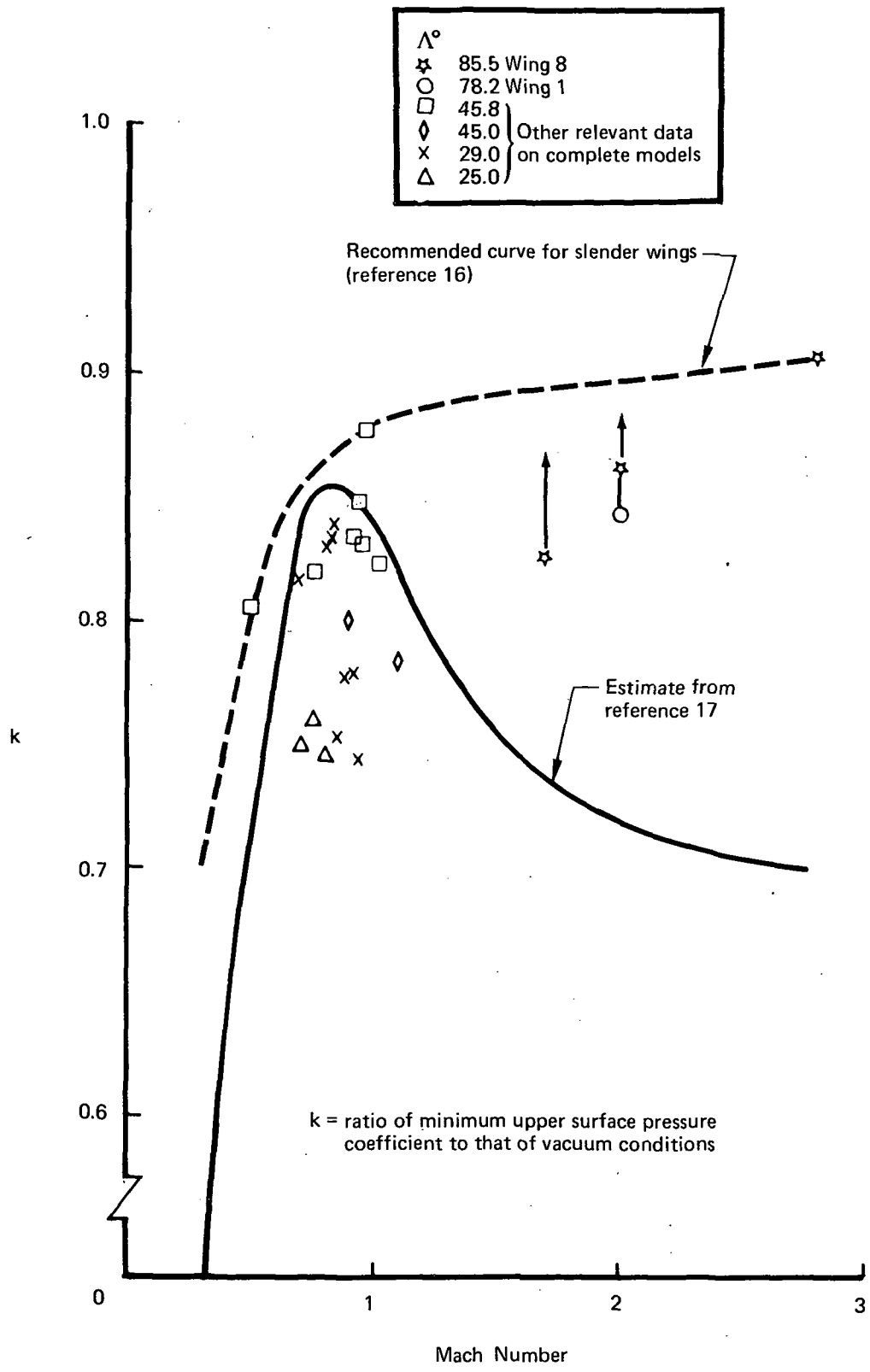

FIGURE 4.4-11.– MINIMUM ATTAINABLE PRESSURE COEFFICIENTS (FROM REF. 16)

against the limit pressure coefficient. If the limit is exceeded, the calculated lifting pressure coefficient is adjusted to a level which causes the total upper surface pressure coefficient to match the limit value.

Comparisons of the "limiter" calculations with measured force and pressure coefficient data are presented in figures 4.4-12 through 4.4-16 for 2 arrow wings of references 1 and 2. Both were 70° sweptback wings, having 3 percent biconvex airfoils, and wing design lift coefficients of 0 (flat) and .08.

The basic thickness pressure comparison is shown in figure 4.4-12. Comparisons of upper and lower surface pressure coefficients at lifting conditions of $C_L \approx .13$ and .25 are shown in figures 4.4-13 and 4.4-14. In the case of the flat wing (figure 3.4.12), several fractions of vacuum pressure coefficient are illustrated; the C_L = .08 wing data are shown for .7 vacuum limiting only.

The limiter feature exhibits considerable improvement in the detail pressure coefficient comparisons over unlimited linear theory as C_L increases.

Force coefficient comparisons for the two wings are shown in figures 4.4-15 and 4.4-16. Pressure limiting at approximately .7 vacuum improves the comparisons appreciably at the higher C_L values.

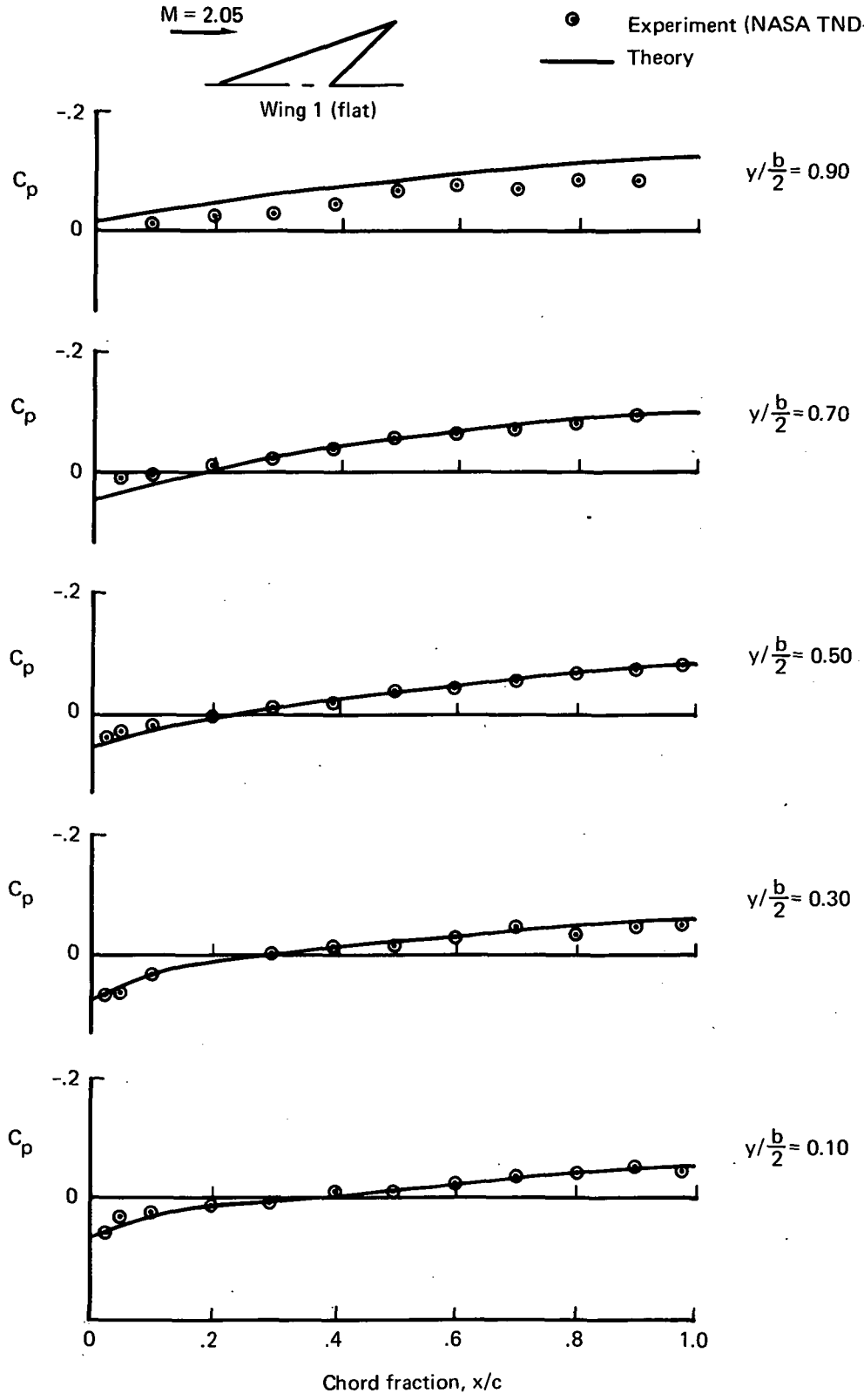

FIGURE 4.4-12.– THICKNESS PRESSURE COMPARISON (C_p DUE TO THICKNESS ONLY)

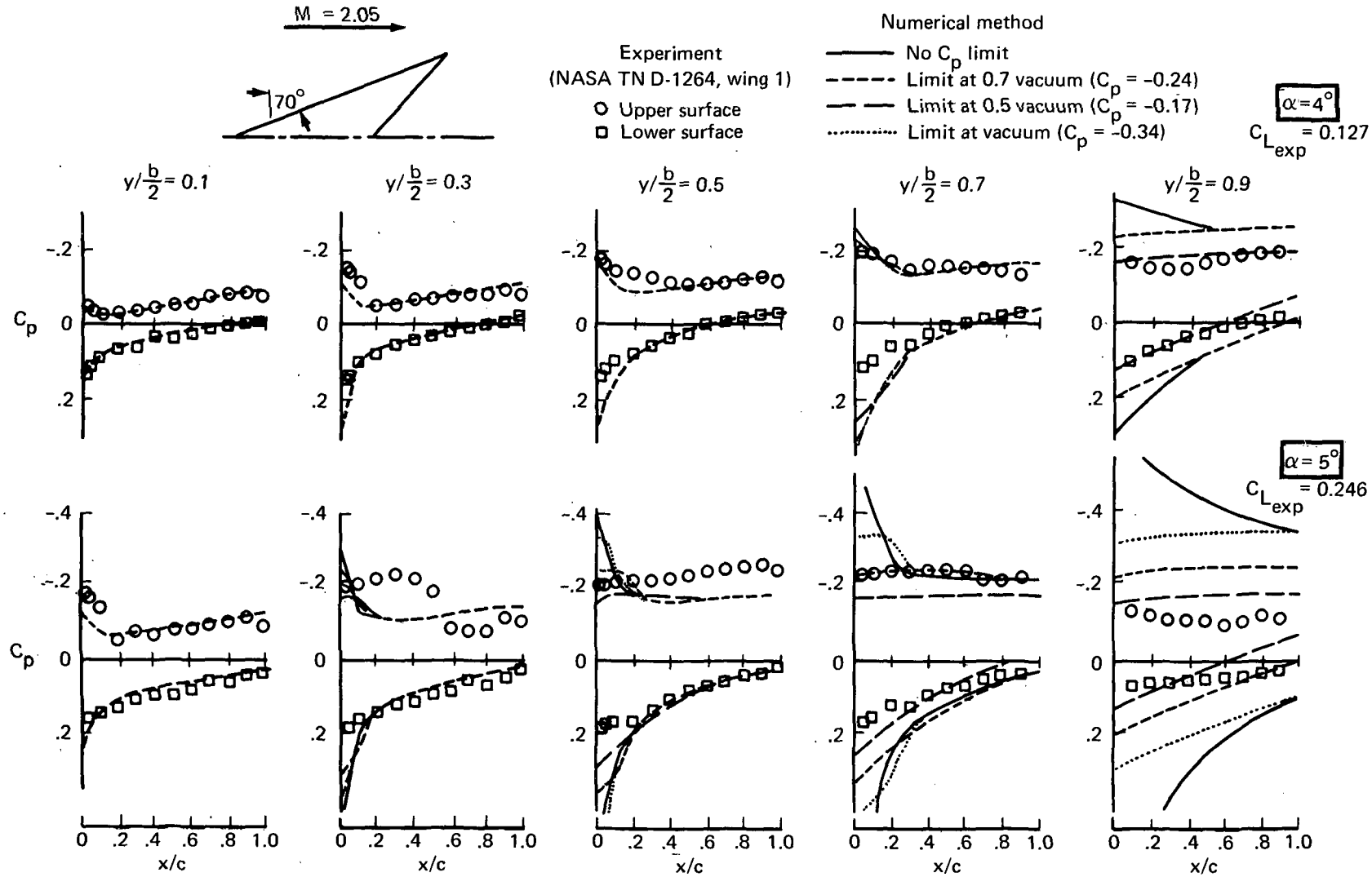

FIGURE 4.4-13.—PRESSURE COEFFICIENT COMPARISON, WING 1 (FLAT WING)

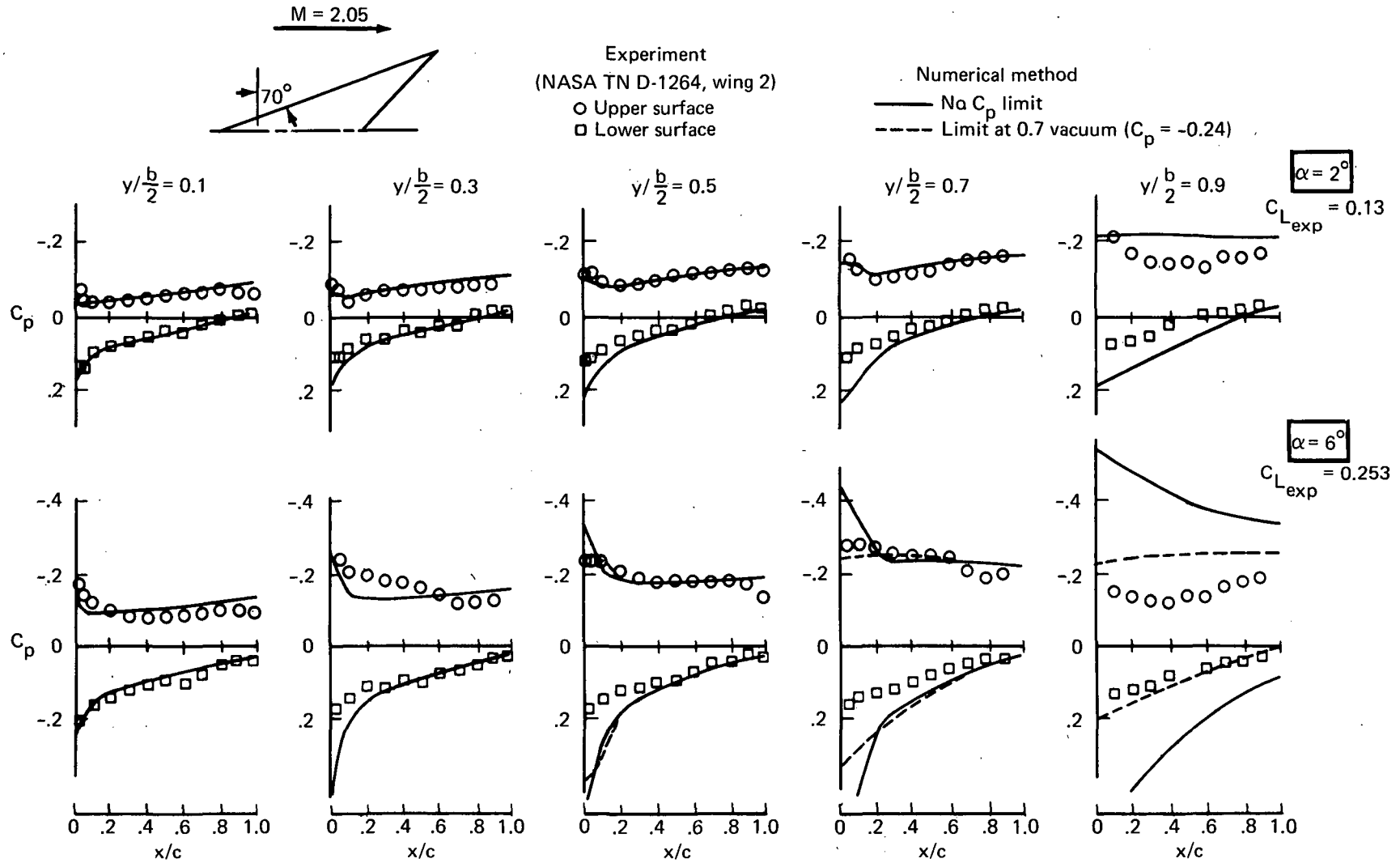

FIGURE 4.4-14.—PRESSURE COEFFICIENT COMPARISON, WING 2 (TWISTED AND CAMBERED WING, DESIGN C_L = .08)

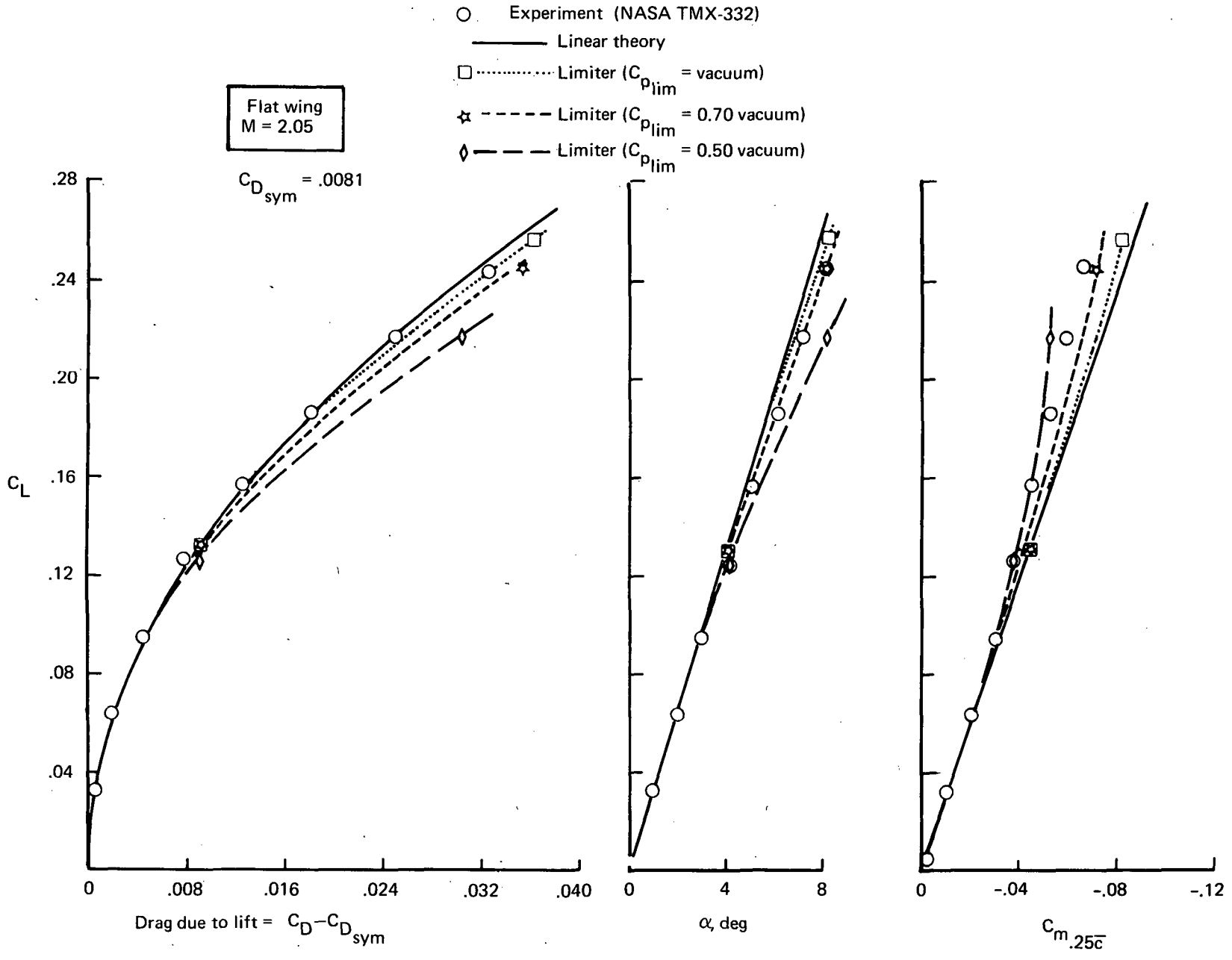

FIGURE 4.4-15.—TEST-THEORY COMPARISON, WING 1 (FLAT WING)

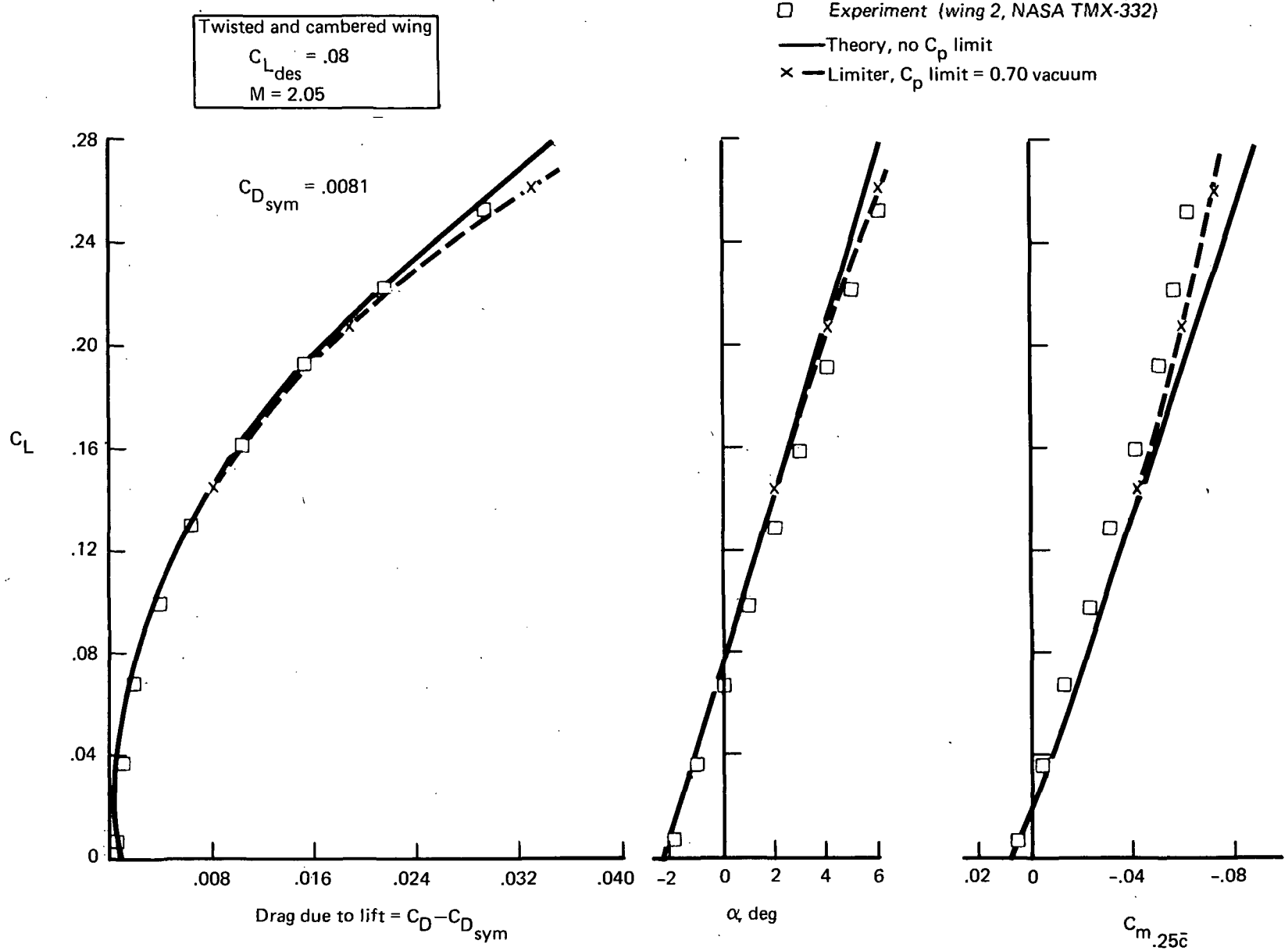

FIGURE 4.4-16 – TEST–THEORY COMPARISON, WING 2 ($C_{L_{des}}$ = 0.08)

5.0 INTERACTIVE GRAPHICS

Interactive graphics for use with the design and analysis system are optional, employing the NASA-LRC cathode ray tube (CRT) display and associated software. Use of the graphics option is requested by an executive control card (described in part 2, user's manual).

The principal uses of the graphics routines in the design and analysis system are to display the configuration, edit input geometry, and to display and/or alter the basic program calculations. Limited capability to redirect the system calculation sequence is available from the CRT console during program execution.

The CRT display and program coding for the interactive graphics setup are based on the NASA-LRC system. However, all display portions of the coding are subroutined or overlaid from the basic programs, so that the system could be readily converted to other CRT arrangements.

Details of the interactive graphics portion of the design and analysis system are given in part 2 (user's manual).

Page Intentionally Left Blank

6.0 REFERENCES

1. Carlson, Harry W. and Harris, Roy V., Jr.: A Unified System of Supersonic Aerodynamic Analysis. NASA SP-228, No. 27, pp. 639-658, 1969.

2. Sommer, Simon C. and Short, Barbara J.: Free Flight Measurements of Turbulent Boundary Layer Skin Friction in the Presence of Severe Aerodynamic Heating at Mach Numbers from 2.8 to 7.0. NACA TN 3391, 1955.

3. Harris, Roy V., Jr: An Analysis and Correlation of Aircraft Wave Drag. NASA TM X-947, 1963.

4. Von Karman, Theodore: The Problem of Resistance in Compressible Fluids. R. Accad. d'Italia, Cl. Sci. Fis., Mat. e Nat., Vol. XIII, 1935, pp. 210-265.

5. Sheppard, L. M.: Methods for Determining the Wave Drag of Non-Lifting Wing Body Combinations. ARC Technical Report R&M No. 3077, 1958.

6. Lighthill, M. J.: Supersonic Flow Past Slender Bodies of Revolution, the Slope of Whose Meridian Section is Discontinuous. Quarterly Journal of Mechanics and Applied Mathematics I, 90, 1948.

7. Whitham, G. B.: The Flow Pattern of a Supersonic Projectile. Communications on Pure and Applied Mathematics. Vol. V, No. 3, August 1952, pp. 301-348.

8. Middleton, W. D. and Carlson, H. W.: A Numerical Method for Calculating Near-Field Sonic Boom Pressure Signatures. NASA TN D-3082, 1965.

9. Carlson, Harry W. and Middleton, W. D.: A Numerical Method for the Design of Camber Surfaces of Supersonic Wings with Arbitrary Planforms. NASA TN D-2341, 1964.

10. Sorrells, Russell and Miller, David S., A Numerical Method for Design of Minimum Drag Supersonic Wing Camber with Constraints on Pitching Moment and Surface Deformation. NASA TN D-7097, 1972.

11. Middleton, W. D. and Carlson, Harry W.: A Numerical Method for Calculating the Flat Plate Pressure Distributions on Supersonic Wings of Arbitrary Planform. NASA TN D-2570, 1965.

12. Carlson, Harry W. and Miller, David S.: Numerical Methods for the Design and Analysis of Wings at Supersonic Speeds. NASA TN D-7713, 1974.

13. Lomax, Howard; Heaslet, Max A.; and Fuller, Franklyn B.: Integrals and Integral Equations in Linearized Wing Theory. NACA Report 1054, 1950.

14. Grant, Frederick C.: The Proper Combination of Lift Loadings for Least Drag on a Supersonic Wing. NACA Report 1275, 1956.

15. Sears, W. R. (Editor): Princeton Series, High Speed Aerodynamics and Test Propulsion, Vo. VI, page 239.

16. Fellows, K. A. and Carter, E. C.: Results and Analysis on Two Isolated Slender Wings and Slender Wing-Body Combinations at Supersonic Speeds. Part 1 - Analysis. ARC C.P. 1131, 1970.

17. Rolf, E. F.: Note on the Maximum Attainable Suction on a Body in an Airstream. ARC 16062, 1953.

NATIONAL AERONAUTICS AND SPACE ADMINISTRATION
WASHINGTON, D.C. 20546

OFFICIAL BUSINESS
PENALTY FOR PRIVATE USE $300

SPECIAL FOURTH-CLASS RATE
BOOK

POSTAGE AND FEES PAID
NATIONAL AERONAUTICS AND
SPACE ADMINISTRATION
451

U.S.MAIL

POSTMASTER: If Undeliverable (Section 158 Postal Manual) Do Not Return

"The aeronautical and space activities of the United States shall be conducted so as to contribute . . . to the expansion of human knowledge of phenomena in the atmosphere and space. The Administration shall provide for the widest practicable and appropriate dissemination of information concerning its activities and the results thereof."

—NATIONAL AERONAUTICS AND SPACE ACT OF 1958

NASA SCIENTIFIC AND TECHNICAL PUBLICATIONS

TECHNICAL REPORTS: Scientific and technical information considered important, complete, and a lasting contribution to existing knowledge.

TECHNICAL NOTES: Information less broad in scope but nevertheless of importance as a contribution to existing knowledge.

TECHNICAL MEMORANDUMS: Information receiving limited distribution because of preliminary data, security classification, or other reasons. Also includes conference proceedings with either limited or unlimited distribution.

CONTRACTOR REPORTS: Scientific and technical information generated under a NASA contract or grant and considered an important contribution to existing knowledge.

TECHNICAL TRANSLATIONS: Information published in a foreign language considered to merit NASA distribution in English.

SPECIAL PUBLICATIONS: Information derived from or of value to NASA activities. Publications include final reports of major projects, monographs, data compilations, handbooks, sourcebooks, and special bibliographies.

TECHNOLOGY UTILIZATION PUBLICATIONS: Information on technology used by NASA that may be of particular interest in commercial and other non-aerospace applications. Publications include Tech Briefs, Technology Utilization Reports and Technology Surveys.

Details on the availability of these publications may be obtained from:

SCIENTIFIC AND TECHNICAL INFORMATION OFFICE

NATIONAL AERONAUTICS AND SPACE ADMINISTRATION

Washington, D.C. 20546